bioRxiv preprint doi: https://doi.org/10.1101/720920. The copyright holder for this preprint (which was not peer-reviewed) is the author/funder. It is made available under a CC-BY-NC 4.0 International license.

1 # Myogenesis modelled by human pluripotent stem cells uncovers
2 # Duchenne muscular dystrophy phenotypes prior to skeletal muscle
3 # commitment

4 Virginie Mournetas[1*], Emmanuelle Massouridès[2], Jean-Baptiste Dupont[1], Etienne Kornobis[3], Hélène Polvèche[2],
5 Margot Jarrige[2], Maxime R. F. Gosselin[4]; Antigoni Manousopoulou[5], Spiros D. Garbis[6]; Dariusz C. Górecki[4,7];
6 Christian Pinset[8]

7 [*] Correspondence: contact@virginie-mournetas.fr

8 [1]INSERM UEVE UMR861, I-STEM, AFM, 28 rue Henri Desbruères, 91100 Corbeil-Essonnes, France

9 [2]CECS, I-STEM, AFM, 28 rue Henri Desbruères, 91100 Corbeil-Essonnes, France

10 [3]Institut Pasteur, 25-28 Rue du Dr Roux, 75015 Paris, France

11 [4]Molecular Medicine, School of Pharmacy and Biomedical Sciences, University of Portsmouth, PO1 2DT,
12 Portsmouth, UK

13 [5]Department of Immuno-Oncology, Beckman Research Institute, City of Hope National Medical Center, Duarte,
14 CA, 91010, USA

15 [6]Proteome Exploration Laboratory, Beckman Institute, California Institute of Technology, Division of Biology
16 and Biological Engineering, 1200 E. California Blvd., MC 139-74, Pasadena, California, 91125, USA

17 [7]Military Institute of Hygiene and Epidemiology, Warsaw, Poland

18 [8]CNRS, I-STEM, AFM, 28 rue Henri Desbruères, 91100 Corbeil-Essonnes, France

bioRxiv preprint doi: https://doi.org/10.1101/720920. The copyright holder for this preprint (which was not peer-reviewed) is the author/funder. It is made available under a CC-BY-NC 4.0 International license.

19 **ABSTRACT**

20 Duchenne muscular dystrophy (DMD) causes severe disability of children and death of young men, with an
21 incidence of approximately 1/5,000 male births. Symptoms appear in early childhood, with a diagnosis made
22 around 4 years old, a time where the amount of muscle damage is already significant, preventing early
23 therapeutic interventions that could be more efficient at halting disease progression. In the meantime, the
24 precise moment at which disease phenotypes arise – even asymptomatically – is still unknown. Thus, there is a
25 critical need to better define DMD onset as well as its first manifestations, which could help identify early
26 disease biomarkers and novel therapeutic targets.

27 In this study, we have used human induced pluripotent stem cells (hiPSCs) from DMD patients to model
28 skeletal myogenesis, and compared their differentiation dynamics to that of healthy control cells by a
29 comprehensive multi-omic analysis. Transcriptome and miRnome comparisons combined with protein
30 analyses at 7 time points demonstrated that hiPSC differentiation 1) mimics described DMD phenotypes at the
31 differentiation endpoint; and 2) homogeneously and robustly recapitulates key developmental steps -
32 mesoderm, somite, skeletal muscle - which offers the possibility to explore dystrophin functions and find
33 earlier disease biomarkers.

34 Starting at the somite stage, mitochondrial gene dysregulations escalate during differentiation. We also
35 describe fibrosis as an intrinsic feature of skeletal muscle cells that starts early during myogenesis. In sum, our
36 data strongly argue for an early developmental manifestation of DMD whose onset is triggered before the
37 entry into the skeletal muscle compartment, data leading to a necessary reconsideration of dystrophin
38 functions during muscle development.

bioRxiv preprint doi: https://doi.org/10.1101/720920. The copyright holder for this preprint (which was not peer-reviewed) is the author/funder. It is made available under a CC-BY-NC 4.0 International license.

39 **INTRODUCTION**

40 Duchenne muscular dystrophy (DMD) is a rare genetic disease, but it is the most common form of myopathy
41 affecting approximately one in 5,000 male births and very rarely female. In this recessive X-linked monogenic
42 disorder, mutations in the *DMD* gene lead to the loss of functional dystrophin protein, resulting in a
43 progressive - yet severe - muscle wasting phenotype (1). In patients, symptoms usually appear in early
44 childhood (2-5 years old) and worsen with age, imposing the use of wheelchair before 15 and leading to
45 premature death by cardiac and/or respiratory failure(s) mostly around 30 years of age (2).

46 At the age of diagnosis (around 4 years old), muscles of DMD patients have already suffered from the
47 pathology (3,4). Several reviews pointed out the limitations of current disease biomarkers, which fail to detect
48 the development of DMD specifically and at an early age (5,6). Meanwhile, no treatment is available to stop
49 this degenerative disease yet. Developing therapies aim at restoring the expression of dystrophin in muscle
50 cells but, so far, the level stays too low to be beneficial to patients (7). The absence of both reliable biomarkers
51 and effective therapies stress the need of better defining the first steps of DMD in humans to be able to
52 increase diagnosis sensitivity and, therefore, improve patient management by accelerating their access to
53 better healthcare as well as develop alternative therapeutic approaches by finding targets that compensate
54 the lack of dystrophin and complement current attempts at restoring its expression (8).

55 In 2007, a seminal publication reported that the gene expression profile of muscles from asymptomatic DMD
56 children younger than 2 years old is already distinguishable from healthy muscles, suggesting that DMD
57 molecular dysregulations appear before disease symptomatic manifestations (4). Evidence obtained in
58 multiple animal models, such as neonatal *GRMD* dogs (9), DMD zebrafish (10) and *mdx* mouse embryos (11), as
59 well as in human foetuses (12–14) even suggest that DMD starts before birth, during prenatal development.
60 Our team recently identified the embryonic dystrophin isoform Dp412e expressed in early mesoderm-
61 committed cells (15), another indication that DMD can start *in utero*. Further exploring DMD onset in human
62 foetuses is extremely challenging for obvious ethical and practical reasons. A way to overcome these issues is
63 to develop a human DMD model *in vitro*, recapitulating embryonic development from human pluripotent stem
64 cells to skeletal muscle lineage.

bioRxiv preprint doi: https://doi.org/10.1101/720920. The copyright holder for this preprint (which was not peer-reviewed) is the author/funder. It is made available under a CC-BY-NC 4.0 International license.

65 To our knowledge, none of the existing human DMD *in vitro* models, either based on tissue-derived myoblasts
66 (16) or on the differentiation of induced pluripotent stem cells (17–21), have been used for studying DMD
67 during the ontogeny of the skeletal muscle lineage. Moreover, original protocols for *in vitro* myogenesis from
68 human pluripotent stem cells (reviewed in (22)) use transgene overexpression or/and cell sorting procedures,
69 and thereby, miss the steps preceding skeletal muscle commitment, *e.g.* paraxial mesoderm and myotome.
70 Novel protocols have recently used transgene-free directed differentiation to recapitulate human embryonic
71 development in a dish, giving theoretical access to the developmental steps (19,23–25).

72 Using one of these protocols (23), we compared the myogenic differentiation dynamics of healthy and DMD
73 hiPSCs using a multi-omic approach to identify early disease manifestations *in vitro*. DMD cells showed marked
74 transcriptome dysregulations from day 10, before the detection of skeletal muscle regulatory factors at day 17.
75 Specifically, we identified the dysregulation of mitochondrial genes as one of the earliest detectable
76 phenotypes. These alterations escalated over the course of muscle specification. In addition, we showed an
77 early induction of Sonic hedgehog signalling pathway, followed by collagens as well as fibrosis-related genes
78 suggesting the existence of an intrinsic fibrotic process solely driven by DMD muscle cells. Overall, our data
79 highlight that human pluripotent stem cells are a suitable cell model to study the ontogeny of skeletal muscle
80 lineage in both healthy and disease conditions. In the context of DMD, they strongly argue for the existence of
81 early disease manifestations during somite development.

82 **RESULTS**

83 To establish the early/developmental impact of *DMD* gene mutations, human induced pluripotent stem cells
84 (hiPSCs) from three DMD patients and three healthy individuals were generated as described previously (15).
85 These cells were subjected to a standardised differentiation protocol without utilisation of feeder cells, cell
86 sorting or gene overexpression resulting in elongated and plurinucleated myotubes within 25 days (23), with
87 an amplification fold of 2918 ± 480 (mean ± SEM). Skeletal muscle progenitor cells after 10 and 17 days of
88 differentiation could be cryopreserved (Figure S1A). Whole transcriptome and miRnome profiles were
89 compared at 7 differentiation time points (tissue-derived myoblasts and myotubes, as well as hiPSC-derived
90 cells at days 0, 3, 10, 17 and 25) and complemented by TMT proteomics and Western blot analyses (Table S1).

bioRxiv preprint doi: https://doi.org/10.1101/720920. The copyright holder for this preprint (which was not peer-reviewed) is the author/funder. It is made available under a CC-BY-NC 4.0 International license.

91 **DMD is initiated prior to the expression of skeletal muscle markers**

92 First, the expression profile of the *DMD* variants was studied by RT-qPCR in healthy and DMD hiPSCs during the
93 differentiation process described in Figure S1A. The *Dp427m* variant, which is normally observed in muscle
94 cells (26), appeared from day 3 and was increased at day 17, in contrast with *Dp412e* – the embryonic variant
95 of dystrophin present in mesoderm cells (15) – which was expressed from day 0, increased at differentiation
96 day 3 and disappeared from day 10. Therefore, the expression of the *DMD* locus is initiated in the very first
97 steps of the differentiation protocol, well before the entry into the skeletal muscle lineage. The ubiquitous
98 variant *Dp71-40* was detected at every time points, in contrast with *Dp116* (Schwann cell variant (27)), *Dp140*
99 (kidney and foetal brain variant (28)) *Dp427p1p2* (Purkinje cell variant (29)), and *Dp427c* which were either
100 undetected or expressed at very low levels (Figure S1B). Interestingly, *Dp260* (retinal variant (30)) followed a
101 similar expression pattern than *Dp427m*.

102 A strong correlation in the transcriptomic data was observed by mRNA-seq and miRNA-seq between samples
103 collected at an individual time point, as opposed to samples from two distinct time points. In addition, the
104 correlation coefficient between samples taken at two successive time points increased as differentiation
105 progressed (Figure 1A). Differential expression analysis in healthy controls between two successive collection
106 days (days 3/0, days 10/3, days 17/10, days 25/17) showed that the proportion of regulated genes decreased
107 from 26 % to 18 % of the whole transcriptome through the course of differentiation (8080 to 5320 mRNAs,
108 adjusted p-value ≤ 0.01, Figure S2A). These observations demonstrate the robustness of the differentiation
109 protocol and are in agreement with an early specialisation and a later refinement of the transcriptome as cells
110 quickly exit pluripotency and become progressively restricted to the skeletal muscle lineage.

111 To characterise the developmental stages achieved by the cells, the expression of lineage-specific markers
112 (both mRNAs and miRNAs) was determined at each time point, together with gene ontology enrichment
113 analyses (Figure 1B-2A, Figure S2B-C, Table S2).

114 Pluripotency was similarly maintained in healthy and DMD cells at day 0 (Figure 2A, Table S2), as already
115 shown by our group (15). At day 3, cells lost pluripotency and became paraxial mesoderm cells expressing
116 marker genes such as *PAX3* and *PAX7* (11) (Figure 2A, Table S2). Importantly, markers of lateral plate (*e.g.*
117 *GATA4* (31)) and intermediate mesoderm (*e.g. PAX8* (32)) were not upregulated at this stage (Table S2).

bioRxiv preprint doi: https://doi.org/10.1101/720920. The copyright holder for this preprint (which was not peer-reviewed) is the author/funder. It is made available under a CC-BY-NC 4.0 International license.

118 Similarly, earlier markers of primitive streak (*e.g. TBX6* (33)), mesendoderm (*e.g. MIXL1* (34)), as well as
119 markers of the other germ layers, endoderm (*e.g. SOX17* (35)) and ectoderm (*e.g. SOX2* (36)) were either not
120 expressed, greatly downregulated or expressed at very low levels (Table S2), suggesting cell homogeneity in
121 the differentiation process.

122 At that early time point, DMD-associated gene dysregulation represented less than 3 % of the entire
123 transcriptome (adjusted p-value ≤ 0.05, Figure 2B) but already contained genes important for development
124 (*e.g. MEIS2* (37)) and muscle formation (*e.g. ACTA1* (38)). However, mesoderm markers were not significantly
125 dysregulated, attesting that mesoderm commitment was mostly unimpaired (Figure 2A, Table S2). No increase
126 in the expression of primitive streak, mesendoderm, endoderm or ectoderm markers was detected, suggesting
127 no differences in the differentiation process of DMD cells at that stage (Table S2).

128 In contrast, a sharp increase in the proportion of dysregulated genes appeared at day 10, mostly including
129 gene downregulations (DMD/Healthy expression ratio ≤ 0.76, adjusted p-value ≤ 0.05). This concerned almost
130 10 % of the transcriptome at day 10 (against 3 % at day 3) and remained stable from 10 to 12 % (1226 mRNAs)
131 until day 25 (Figure 2B). At day 10, healthy cells expressed genes typically observed during somitogenesis, such
132 as *PAX3* (39) *NR2F2* (40), *PTN* (41), *MET* (42), *H19* and *IGF2* (43) (Table S2). More precisely, their transcriptome
133 exhibits a mixed profile between dermomyotome (expression of *GLI3* (44) and *GAS1* (45) but not *ZIC3* (46)) and
134 myotome (expression of *MET* (47) and *EPHA4* (48) but not *LBX1* (49)) (Table S2). Neither markers of presomitic
135 mesoderm cells (*e.g. FGF8* (50)) and neural plate cells (*FOXD3* (51)), nor markers of sclerotome (*e.g. PAX1* (52))
136 and dermatome (*e.g. EGFL6* (53)) were upregulated (Table S2) in both healthy and DMD cells. In the meantime,
137 several somite markers were downregulated, including *H19, IGF2*, *MET* and *SEMA6A* (54) (validated at the
138 protein level for SEMA6A, Figure 2A-S3A, Table S2), while a slight upregulation of chondrocyte markers was
139 highlighted and confirmed at the protein level for GLI3 (Figure S3B), together with a significant enrichment of
140 the gene ontology term ‘nervous system development’, suggesting potential lineage bifurcations at day 10
141 (Figure 2A-S2C, Table S2).

142 The study of differentiation dynamics presented above highlights that mesoderm commitment is not impaired
143 by the absence of dystrophin, and shows that DMD onset takes place at the somite cell stage, before the
144 expression of the skeletal muscle program and especially before the upregulation of *Dp427m* expression.

bioRxiv preprint doi: https://doi.org/10.1101/720920. The copyright holder for this preprint (which was not peer-reviewed) is the author/funder. It is made available under a CC-BY-NC 4.0 International license.

145 **DMD skeletal muscle progenitor cells exhibit specific muscle gene dysregulations**

146 Healthy and DMD cells were in the skeletal muscle compartment at day 17, as evidenced by the expression of
147 multiple lineage-specific genes, such as transcription factors (*e.g. MYOD1* (55)), cell surface markers (*e.g.*
148 *CDH15* (56)), sarcomere genes (*e.g. TNNC2* (57)), dystrophin-associated protein complex (DAPC) genes (*e.g.*
149 *SGCA* (58)), Calcium homeostasis genes (*e.g. RYR1* (59)) and muscle-specific miRNAs (myomiR, *e.g. MIR1-1*
150 (60)). This was also observed at the protein level for CDH15, TNNC2 and RYR1 (Figure 1B, Table S2). They both
151 showed an embryonic/foetal phenotype characterised by *ERBB3* expression, in contrast with tissue-derived
152 myoblasts that expressed *NGFR* (21). Here again, alternative cell lineages were absent or greatly
153 downregulated, such as tenocytes (*e.g. MKX* (61)), chondrocytes (*e.g. SOX5* (62)), osteoblasts (*e.g. SPP1* (63))
154 or nephron progenitors (*e.g. SALL1* (64)) (Table S2).

155 Interestingly, DMD cells did not show a significant dysregulation of skeletal muscle transcription factors (Table
156 S2). However, several myomiRs were found downregulated (*e.g. MIR1-1*, Figure 2C), together with genes
157 related to calcium homeostasis (*e.g. ATP2A2* (65), at both mRNA and protein level, Figure 2D-E) as well as
158 members of the DAPC (*e.g. SNTA1* (66)) (Table S2). Concerning cell lineages, there was no visible difference
159 when compared to healthy controls, except an upregulation of markers associated with chondrocytes, which
160 was confirmed at the protein level for GLI3 (Figure S3C), and a significant enrichment of the gene ontology
161 term ‘nervous system development’ previously seen at day 10, together with ‘kidney development’ and
162 ‘ossification’ (Figure 2A-S2C, Table S2).

163 DMD-specific dysregulations were further queried at the protein level using TMT proteomics. 3826 proteins
164 were detected in the 6 processed samples (3 healthy and 3 DMD, Table S3). Among these list, 185 proteins
165 (139 + 46) were found significantly dysregulated in DMD and 375 (329 + 46) of the corresponding mRNAs were
166 previously detected dysregulated in the RNA-seq analysis, the overlap between protein and mRNA identified
167 dysregulations being 46 ($|\text{log2FoldChange}| \geq 0.4$ and adjusted p-value ≤ 0.05, Figure S3D-E, Table S4).
168 Moreover, among the total of 514 genes represented in Figure S3F, 98 were dysregulated alike in both
169 datasets (56 upregulated + 42 downregulated) against 13 (12 + 1) in the opposite direction ($|\text{log2FoldChange}|$
170 ≥ 0.4, Figure S3F, Table S4) resulting in a Spearman correlation of $r = 0.49$ and p-value < 0.0001. In this
171 mRNA/protein comparison, the mRNA experiment was more sensitive than protein experiment and could also
172 be considered as a good proxy for proteins.

bioRxiv preprint doi: https://doi.org/10.1101/720920. The copyright holder for this preprint (which was not peer-reviewed) is the author/funder. It is made available under a CC-BY-NC 4.0 International license.

173 To better characterise the most direct consequences of the loss of *DMD* in muscle cells, *DMD* expression was
174 knocked-down at day 17 by transient exon skipping using a specific phosphorodiamidate morpholino oligomer
175 targeting *DMD* exon 7 (PMO7) in a healthy hiPSC line. Treatment with PMO7 resulted in significant exon
176 skipping which was correlated with reduced *DMD* expression up to 94% (Spearman r = -0.88, analysed pairs =
177 59, p-value < 0.0001, Figure S4A) and reduced dystrophin protein levels (up to 81%, Figure S4B). In parallel, the
178 expression of specific transcripts was measured by RT-qPCR the 3 following days (Figure S4A): transcripts
179 coding for *MYH3*, *MYOG* and *SGCA* were significantly downregulated after PMO7 treatment (gene group 1),
180 while transcripts coding for *DES* and *ITGA7* were not affected (gene group 2).

181 Therefore, DMD cells efficiently enter the skeletal muscle compartment at day 17, but exhibit dysregulations in
182 several features typically associated with dystrophic muscles, which could be a consequence of the early
183 manifestations of DMD detected at day 10. Some of these identified dysregulations were mimicked by
184 transient *DMD* knockdown.

185 **hiPSC differentiation leads to embryonic/foetal myotubes that reproduce DMD phenotypes**

186 As previously described (23), both healthy and DMD hiPSC-derived myotubes (day 25) were able to twitch
187 spontaneously in culture, and fluorescent staining of nuclei and α-actinin confirmed cell fusion and the
188 formation of striation patterns typical of muscle fibres *in vivo* (Figure 3A). Western blot analyses on protein
189 extracts from DMD cells confirmed that dystrophin was either undetectable or slightly expressed (Figure 3B),
190 as in the corresponding patient muscle biopsies (data not shown).

191 We selected representative mRNAs and miRNAs and showed that both hiPSC-derived and tissue-derived
192 myotubes have exited the cell cycle and upregulated genes expressed in skeletal muscles (Figure S5A, Figure
193 4A, Table S2). This included skeletal muscle myomiRs (*MIR1-1*, *MIR133* and *MIR206* (67,68)), transcription
194 factors involved in skeletal myogenesis including those of the muscle regulatory factor (MRF) family (*e.g.*
195 *MYOD1* (55), *MYOG* (69)), specific muscle cell surface markers (*e.g. CDH15* (56), *ITGA7* (70)) as well as genes
196 involved in the formation of the DAPC (*e.g. SGCA* (58), *DTNA* (71)), sarcomeres (*e.g. TNNC2* (57), *TNNT3* (72)),
197 myofibril organisation (*e.g. UNC45B* (73), *NACA* (74)) and the triggering of excitation-contraction coupling at
198 the neuromuscular junction (NMJ, *e.g. MUSK* (75), *DOK7* (76)) (Figure 4A, Table S2).

bioRxiv preprint doi: https://doi.org/10.1101/720920. The copyright holder for this preprint (which was not peer-reviewed) is the author/funder. It is made available under a CC-BY-NC 4.0 International license.

199 Even though global analysis showed that hiPSC-derived myotubes were similar to their tissue-derived
200 counterparts in term of lineage commitment, they displayed an embryonic/foetal phenotype – as suggested in
201 progenitors at day 17. This can be illustrated by the expression of the embryonic/foetal myosin heavy/light
202 chains *MYH3* (77), *MYH8*(78), *MYL4* (79) and *MYL5* (80) but not the postnatal transcripts *MYH1* and *MYH2* (81),
203 which were detected in tissue-derived myotubes. Myotubes derived from hiPSCs had also higher levels of *IGF2*,
204 which is downregulated at birth (82), and expressed *DLK1*, which is known to be extinct in adult muscles (83)
205 (Figure S5B).

206 Despite the embryonic/foetal phenotype, hiPSC-derived myotubes showed evidence of terminal
207 differentiation and cellular maturation. First, their total level of myosin heavy chain proteins was significantly
208 higher than in tissue-derived myotubes, as confirmed by Western blotting (Figure 3B). RNAs and proteins
209 involved in DAPC formation (*e.g.* DMD, SGCA (58) and SGCG (84)), as well as in excitation-contraction coupling
210 (*e.g.* RYR1 (59) and CACNA1S / CAV1.1 (85)) were also present at higher levels (Figure 3B-4A). Finally, higher
211 expression of skeletal muscle transcription factors (*e.g. MEF2C* (86)), and of multiple genes involved in muscle
212 contraction (*e.g. TNNT3* (72)), NMJ formation (*e.g. RAPSN* (87)), and creatine metabolism (*e.g. CKM* (88))
213 indicates that hiPSC-derived cells expressed features of fully differentiated muscle cells (Figure 4A). Similar to
214 previous time points, day 25 cells were negative for markers of alternative muscle lineages, *i.e.* cardiac
215 (*MIR208a* (89), *MYL7* (90) and *RYR2* (91)) and smooth muscle cells (*MYH11* (92), *CNN1* (93) and *CHRNA3/B2/B4*
216 (94))(Table S2).

217 In DMD cells, unbiased mRNA-seq analysis highlighted striking transcriptome dysregulations with 3,578
218 differentially expressed genes in hiPSC-derived myotubes including well-known muscle genes. There was a
219 global trend towards downregulation of muscle transcription factors, which was only significant for *MEF2A* and
220 *MEF2D* in hiPSC-derived myotubes and *EYA4* and *MYOD1* in tissue-derived myotubes (Figure S5C). In addition,
221 myomiRs previously associated with muscle dystrophy (dystromiRs, *e.g. MIR1-1* (60), Figure 2C) were found
222 downregulated (Table S2). Similarly, a global downregulation phenotype was observed in both tissue- and
223 hiPSC-derived DMD myotubes, and concerned multiple mRNAs and/or proteins associated with known disease
224 phenotypes, such as cell surface markers (*e.g. ITGA7* (70)), DAPC organisation (*e.g.* both SGCA mRNA and
225 protein (58) as well as SGCG protein (84)), myofibril organisation (*e.g. UNC45B* (73)), sarcomere formation (*e.g.*
226 *MYO18B* (95)), NMJ function (*e.g. CHRNB1* (96)) and calcium homeostasis (*e.g. ATP2A2* mRNA (65) and RYR1
227 protein (59)) (Figure 3B for protein data, 4B for transcript data, S2C for enrichment data).

bioRxiv preprint doi: https://doi.org/10.1101/720920. The copyright holder for this preprint (which was not peer-reviewed) is the author/funder. It is made available under a CC-BY-NC 4.0 International license.

228 Then we compared the DMD/Healthy expression ratios at day 25 with two sets of published omics data from
229 healthy and DMD muscle biopsies: one obtained at the mRNA level in pre-symptomatic DMD patients younger
230 than 2 years old (4) and another at the protein level in patients aged from 9 months to 8 years old (97). Both
231 datasets were closer to day 25 cells (hiPSC-derived myotubes) than day 17 cells as expected. Our hiPSC-derived
232 myotubes expressed 250 of the 261 dysregulated genes and 203 of the 226 dysregulated proteins found in
233 these respective studies (Spearman correlations of r = 0.36 and r = 0.42, p-value < 0.0001, Figure 4C, Table S4).
234 Among these, respectively 90 and 63 genes were also significantly dysregulated in our dataset
235 (|log2FoldChange| ≥ 0.4, adjusted p-value ≤ 0.05): 88% (79 / 90 genes) of the identified genes from the mRNA
236 dataset and 78% (49 / 63 genes) of the identified genes from the protein dataset were dysregulated in the
237 same direction, resulting in Spearman correlation of r = 0.45 and r = 0.59 respectively (p-value ≤ 0.0001, Figure
238 4C-D, Table S4).

239 Altogether, these data indicate that hiPSC-derived myotubes recapitulate a full skeletal muscle differentiation
240 program, and exhibit an embryonic/foetal phenotype. Despite that, it shows that DMD phenotypes are already
241 detectable at the transcriptional level and correlated with those found in human patients. This validates the
242 relevance of this cell system to model the DMD pathology.

243 **Markers of fibrosis are intrinsic to DMD hiPSC-derived myotubes**

244 As presented above, the upregulation of chondrocyte markers in DMD cells, although already present at day
245 10, became significant from day 17 (Figure 2A, Table S2). It was accompanied by the upregulations of the Sonic
246 hedgehog (SHH) signalling pathway and of multiple collagens (Figure 5A, Table S2). Genes encoding the *P4H*
247 collagen synthases, were not dysregulated while *RRBP1* (that stimulates collagen synthesis (98)) together with
248 *PLOD1* and *PLOD2* (that stabilise collagens (99,100)) were significantly upregulated. Moreover, *SETD7*, a gene
249 known for activating collagenases (101), was significantly downregulated.
250 At the myotube stage, a fibrosis-related gene set was clearly upregulated in DMD cells, as illustrated by the
251 overexpression of *ANGPT1* (102), *CTGF* (103), collagens (*e.g. COL1A2* (104)), matrix metallopeptidases (*MMPs*)
252 and tissue inhibitors of metallopeptidase (*TIMPs*) (105) (Figure 5B). Conversely, the myomiR *MIR133* that
253 controls *CTGF* expression (106) was repressed (Table S2). Interestingly, gene members of the transforming

bioRxiv preprint doi: https://doi.org/10.1101/720920. The copyright holder for this preprint (which was not peer-reviewed) is the author/funder. It is made available under a CC-BY-NC 4.0 International license.

254 growth factor (TGF)-β pathway, a well-known inducer of fibrosis (107), were not found dysregulated (Figure
255 5B, Table S2).
256 Altogether, these data argue for fibrosis as an intrinsic feature of DMD skeletal muscle cells, rather than a
257 process solely driven by interstitial cell populations in the niche. Furthermore, this muscle-driven fibrosis
258 seems independent of the TGF-β pathway, and could rather depend on the SHH pathway, together with an
259 intrinsic upregulation of chondrocyte markers and collagens.

260 **Genes involved in mitochondrial metabolism are drastically dysregulated in DMD hiPSC-derived myotubes**

261 As previously described (108) and illustrated on Figure S6A, genes involved in the energy metabolism of DMD
262 hiPSC-derived myotubes were dysregulated at the creatine and carbohydrate levels, up to the respiration
263 (Figure 6A-B, Figure S2C, Table S2). The creatine transporter was not impacted while mRNAs coding for
264 enzymes of both creatine and creatine phosphate biosynthesis were underrepresented. Neither glucose nor
265 glutamate transporter expression were impaired. However, genes involved in glutamine biosynthesis (followed
266 by gluconeogenesis that feeds glycolysis from glutamine) as well as glycogenesis (followed by glycogenolysis
267 that feeds glycolysis from glycogen) were all downregulated, together with genes coding for glycolysis itself. In
268 contrast, genes coding for the pentose phosphate pathway (which is in parallel to glycolysis) were upregulated,
269 especially the oxidative part. Gene expression for pyruvate decarboxylation and generation of acetyl-CoA to
270 feed the tricarboxylic acid (TCA) cycle was also impaired. Finally, the genes involved in the TCA cycle itself
271 (Figure 6A, Figure S2C) and the mitochondrial electron transport chain were downregulated Figure 6B, Figure
272 S2C). This is particularly reinforced by lower levels of a member of the ATP synthase complex ATP5A1 at both
273 mRNA and protein levels (Figure 6C-D). These mRNA and protein data were completed by the measurement of
274 ATP levels, which were significantly decreased in DMD hiPSC-derived myotubes (Figure 6E). Moreover,
275 transcripts encoded by the mitochondrial DNA and mitochondrial DNA itself were decreased in DMD hiPSC-
276 derived myotubes at day 25 (Figure S6B-S6E).
277 In the presented cell model, a significant downregulation of a mRNA set coding for mitochondrial proteins was
278 primarily observed at day 10 with the downregulation of 11 % (12 mRNAs, DMD/Healthy expression ratio ≤
279 0.76, adjusted p-value ≤ 0.05) of the mitochondrial outer membrane genes, and amplified during the
280 differentiation of DMD cells (Figure 7A). Therefore, defects depicted at day 25 rooted before the expression of
281 the skeletal muscle program at day 17. Among them, mRNA downregulation of *TSPO*, a channel-like molecule

bioRxiv preprint doi: https://doi.org/10.1101/720920. The copyright holder for this preprint (which was not peer-reviewed) is the author/funder. It is made available under a CC-BY-NC 4.0 International license.

282 involved in the modulation of mitochondrial transition pore (109), occurred from day 10 to day 25. This
283 downregulation was also observed at the protein level at day 17 (Figure 7B). Moreover, the protein import
284 system was affected from day 17 at both mRNA and protein levels (Figure S6C-S6F). Simultaneously, mRNAs
285 involved in mitochondrial genome transcription started to be downregulated, followed by genes involved in
286 mitochondrial DNA replication at day 25 (Figure S6D-S6G). This progressive increase of dysregulations was also
287 observed at the level of the entire mRNA set related to mitochondria (around 1,000 mRNAs) as illustrated by
288 the volcano plots as well as the gene ontology enrichments (Figure 7C, Figure S2C).
289 Our data highlight early impairments in genes coding for mitochondria that start at the somite stage and
290 increase with the differentiation in an orderly manner. These elements complete the mitochondrial DMD
291 phenotype described above at the myotube stage.

292 Altogether, our study demonstrates that DMD starts prior to the expression of well-described markers of
293 muscle differentiation. It shows that hiPSC-based experimental models of DMD can help identify early disease
294 manifestations and stratify multiple pathological features over the course of muscle development.

295 **DISCUSSION**

296 Since the discovery of the *DMD* gene in 1987 (1), DMD cellular phenotypes were considered under the unique
297 scope of a “mechanical hypothesis” in which dystrophin deficiency led to membrane leakage and ultimately
298 muscle cell rupture. However, over the last 15-20 years, studies have brought unequivocal evidence that
299 multiple additional factors are in play, such as calcium intracellular overloads (110,111), excessive oxidative
300 stress (112,113), metabolic switches (114,115), as well as an overall tissue context where aberrant interactions
301 between resident cells lead to inflammation and fibro-adipogenesis (116–118). This has progressively led to a
302 complex picture involving interdependent homeostatic perturbations and to date, the identification of
303 prevalent pathological features driving the initiation of DMD is hardly feasible.

304 The skeletal myogenesis modelled here by the differentiation of hiPSCs, without gene overexpression or cell
305 sorting, homogeneously and robustly recapitulates key developmental steps – pluripotency, mesoderm,
306 somite and skeletal muscle – without any trace of other lineages. Therefore, it is a suitable dynamic model for
307 studying human skeletal muscle development in both healthy and DMD cells, offering the possibility to clarify

bioRxiv preprint doi: https://doi.org/10.1101/720920. The copyright holder for this preprint (which was not peer-reviewed) is the author/funder. It is made available under a CC-BY-NC 4.0 International license.

308 the consequences of the absence of dystrophin at each step of the differentiation process, as well as to
309 explore dystrophin functions and find earlier and more specific disease biomarkers.
310 As previously observed with pluripotent stem cells (119), hiPSC-derived myotubes at day 25 displayed an
311 embryonic/foetal gene expression profile. However, a clear distinction must be made between the nature of
312 the expressed isoforms – embryonic / foetal / postnatal – and the degree of differentiation. For instance,
313 hiPSC-derived myotubes expressed multiple markers of terminally differentiated muscles at levels higher than
314 those measured in tissue-derived myotubes. With the idea of exploring human DMD phenotypes during
315 muscle development, we argued that generating embryonic/foetal myotubes from hiPSCs would not be a
316 limitation.

317 In qualitative terms, DMD hiPSC-derived myotubes showed an overall morphology similar to healthy controls,
318 with cell fusion and clear striation patterns, suggesting that the potential impact of dystrophin during *in vitro*
319 differentiation is subtle and does not prevent myotube formation. However, our unbiased mRNA-seq analysis
320 highlighted striking transcriptome dysregulations at day 25. This includes numerous genes which can be linked
321 to previously described DMD phenotypes such as 1) DAPC dissociation (120); 2) rupture of calcium
322 homeostasis (110); 3) myomiR downregulation (60,121); 4) sarcomere destabilisation (122–124); 5)
323 mitochondrial and metabolism dysregulations (114,115); 6) NMJ fragmentation (125,126) and 7) fibrosis
324 (118,127). It is interesting to note that these phenotypes are already detected at the transcriptional level in
325 embryonic/foetal myotubes, while they usually appear postnatally in human patients and other animal
326 models. In addition, most of them are often considered as consequences of degeneration-regeneration cycles
327 typical of DMD muscles *in vivo* (123,128,129) which are absent in our *in vitro* model, indicating that a part of
328 these defects are primarily due to the absence of dystrophin itself. In particular, our data suggest that fibrosis
329 is an intrinsic feature of DMD skeletal muscle cells, and therefore, it does not absolutely require a specific
330 tissue context or additional cell populations to be detected *in vitro*. Fibrosis is a major hallmark of DMD
331 pathophysiology, and the regulation of this process has been largely investigated in the past (107,130). A long-
332 debated question is the implication of the TGFβ signalling pathway (131). In this study, TGFβ signalling was
333 inhibited up to day 17 by specific molecules contained in the cell culture media, and TGFβ-related genes were
334 not upregulated at day 25, suggesting that the observed upregulation of fibrosis-related markers is TGFβ-
335 independent.

bioRxiv preprint doi: https://doi.org/10.1101/720920. The copyright holder for this preprint (which was not peer-reviewed) is the author/funder. It is made available under a CC-BY-NC 4.0 International license.

336 Since several studies in human patients and animal models had described dystrophic phenotypes in DMD
337 foetuses/infants (9–14), we investigated the precise timing of disease onset in our hiPSC-derived cells. First,
338 the absence of dystrophin does not modify the capacity of cells derived from adult tissue biopsies to be
339 reprogramed using the approach developed by Takeshi and Yamanaka (132). Both healthy and DMD cells
340 retained pluripotency and the capacity to enter the mesoderm compartment at day 3. At that time, the
341 embryonic dystrophin Dp412e is expressed and only marginal dysregulations are observed in DMD cells, *a*
342 *priori* unrelated to cell fate choice as cells only express paraxial mesoderm markers at levels similar to healthy
343 controls.

344 DMD dysregulations are greatly increased at day 10, when cells express somite markers. At that time, we
345 noticed few significant dysregulations of cell lineage markers, which became more prevalent at day 17 and 25.
346 This might be an indication that to some extent, cell fate is misguided in DMD cells, where skeletal muscle
347 markers are underexpressed and replaced by markers of alternative lineages, such as chondrocytes.

348 First visible at day 10, we identified the dysregulation of mitochondrial genes as one of the key processes
349 happening in an orderly manner. Interestingly, early observations prior to the discovery of the *DMD* gene had
350 hypothesised that DMD was a mitochondrial/metabolic disease based on protein quantifications and enzyme
351 activities (114,133). Later, mitochondria was identified as a key organelle in DMD, responsible for metabolic
352 perturbations but also calcium accumulation and generation of reactive oxygen species (110–113). In this
353 study, numerous genes coding for proteins located in the outer mitochondrial membrane start to be
354 downregulated from day 10 in DMD cells, such as the benzodiazepine receptor TSPO, a member of the
355 controversial mitochondrial permeability transition pore (mPTP) (109). The mPTP is a multiprotein complex
356 whose members are not all precisely identified, and several studies suggest that it might be involved in DMD
357 pathophysiology (134,135). A chicken-and-egg question currently debated relates to the initiation of these
358 homeostatic breakdowns, as positive feedbacks exist between mitochondria, oxidative stress and calcium
359 homeostasis dysregulations (111,112). At the transcriptome level, dysregulations of genes controlling calcium
360 homeostasis were detected after day 10, suggesting that mitochondrial impairment starts early and has
361 predominant consequences in DMD, as hypothesised by Timpari *et al*. (108). Further experiments are needed
362 to better evaluate the impact of mitochondrial dysregulations at the functional level.

363 Day 17 marks the entry into the skeletal muscle compartment with the expression of specific transcription
364 factors, cell surface markers, myomiRs as well as the increase of skeletal muscle variant of dystrophin

bioRxiv preprint doi: https://doi.org/10.1101/720920. The copyright holder for this preprint (which was not peer-reviewed) is the author/funder. It is made available under a CC-BY-NC 4.0 International license.

365 (*Dp427m*). It also marks the initiation of the skeletal muscle gene dysregulations observed at the myotube
366 stage (*i.e.* downregulation of genes involved in DAPC and calcium homeostasis). For instance, the upregulation
367 of fibrosis-related genes observed in DMD myotubes at day 25 is already visible at day 17, with the
368 upregulation of the SHH pathway as well as collagen-related genes. In this study, it is seen as an early indicator
369 of DMD physiopathology, confirming previous observations in DMD infants, both transcriptionally (4) and
370 histologically (136,137).

371 Moreover, several myomiRs were found downregulated at days 17 and 25 and seem to play a central part in
372 multiple DMD phenotypes. Beside their role in myogenesis (67,68), myomiRs can be involved in calcium
373 homeostasis (138), metabolism and mitochondrial functions (139,140), and fibrosis (106,141). In particular,
374 *MIR1-1* and *MIR206* are known to target key genes such as *CACNA1C* (138), *CTGF* (106), *RRBP1* (141), several
375 regulators of the pentose phosphate pathway (139), and even transcripts encoded by the mitochondrial
376 genome (140). Even though the functional consequences of the multiple gene and myomiR dysregulations
377 highlighted in this study is virtually impossible to anticipate, we believe that myomiRs can be key players in
378 DMD physiopathology.

379 Few studies argued that DMD starts before the expression of the muscular dystrophin protein (18,142). Our
380 data suggests that *Dp427m* is actually expressed before muscle commitment but at a lower level. This fact
381 might explain why disease phenotypes seem to be initiated at the somite stage. This early initiation could also
382 be explained by the deficit in other dystrophin isoforms expressed before day 10, such as Dp412e at day 3 (15),
383 as well as by the decrease or loss of other RNA products expressed from the *DMD* locus, such as the ubiquitous
384 isoform Dp71-40 or long non-coding RNAs (143). The lack of knowledge around these additional products from
385 the *DMD* locus contrasts with the extensive amount of data on the structure and function of the main
386 muscular isoform Dp427m whose most studied role is to stabilise muscle cell membrane during contraction
387 (144). *DMD* knockdown results at day 17 in a healthy cell line with partial mimicking of DMD phenotype could
388 suggest a dynamic process in DMD: some dysregulations might not be reproduced by removing *DMD* after
389 muscle commitment highlighting the fact that absence of DMD locus expression during development could
390 have impacts before cells becoming muscles and, therefore, before Dp427m having its well-known role in
391 muscles, as it is shown by our multi-omic study. The role of *Dp427m* in non-muscle cells could also be
392 questioned. Other tissue specific isoforms have been described, *e.g.* in the retina (Dp260 (30)) and in the brain

bioRxiv preprint doi: https://doi.org/10.1101/720920. The copyright holder for this preprint (which was not peer-reviewed) is the author/funder. It is made available under a CC-BY-NC 4.0 International license.

393 (Dp427c (145), Dp427p (29) and Dp140 (28)), some of which are also slightly expressed in skeletal muscles
394 under certain circumstances (146), but their role remains mostly unknown. Interestingly, in our data, the
395 expression of Dp260 follows the same pattern of expression as Dp427m. It has been shown that the expression
396 of Dp260 in *mdx*/utrnK/K mice can rescue the *mdx* phenotype (147), indicating overlapping functions between
397 Dp427m and Dp260. On the other hand, it is now well established that a third of DMD patients display
398 cognitive deficiencies – which might be correlated with mutations affecting Dp140 (148) – attesting that
399 dystrophin can be involved in other cell functions.

400 To date, the standard of care for DMD patients helps mitigate and delay some of the most severe symptoms
401 but remains insufficient to have a curative effect. Despite decades of work with the *mdx* mouse model, only a
402 few pharmacological candidate molecules have moved forward to clinical trials, with variable efficiency. As
403 several gene therapy trials have been recently initiated with promising preliminary data, we believe that our
404 human *in vitro* model system might be useful for the development of combination therapies. Recent studies
405 have proved that the association of two different therapeutic approaches could have a synergistic effect on
406 the overall treatment outcome, and can be used for instance to boost the effect of dystrophin re-expression by
407 antisense oligonucleotides or gene therapy (8,149,150). Here, our extensive RNA-seq data could help identify
408 relevant therapeutic targets for pharmacological intervention, such as CTGF – involved in fibrosis and found
409 upregulated in DMD myotubes – which can be inhibited by monoclonal antibodies (151), or TSPO receptor – a
410 receptor potentially member of the mPTP downregulated in DMD cells – targetable with benzodiazepines
411 (152). In addition, our model might also be used as a platform to screen pharmacological compounds in an
412 unbiased high-throughput manner. Indeed, skeletal muscle progenitor cells at day 17 can be robustly
413 amplified, cryopreserved and plated in a 384-well plate format (data not shown). Thus, they could be an
414 interesting tool to highlight pharmacological compounds to be used alone, or in combination with gene
415 therapy.

416 To summarise, the directed differentiation of hiPSCs without gene overexpression or cell sorting
417 homogeneously and robustly recapitulates key developmental steps of skeletal myogenesis and generates
418 embryonic/foetal myotubes without any trace of other lineages. The absence of dystrophin does not
419 compromise cell reprogramming, pluripotency or the entry into the mesoderm compartment. While a very low
420 amount of the long muscular dystrophin isoform is expressed, a significant transcriptome dysregulation can be

bioRxiv preprint doi: https://doi.org/10.1101/720920. The copyright holder for this preprint (which was not peer-reviewed) is the author/funder. It is made available under a CC-BY-NC 4.0 International license.

421 observed at the somite stage that implicates mitochondria prior to dysregulations of genes controlling calcium
422 homeostasis. Despite their ability to enter the skeletal muscle lineage compartment and become myotubes,
423 DMD cells exhibit an imbalance in cell fate choice as they express lower amounts of key muscle proteins and
424 retain basal expression of marker genes from other lineages, leading to the well-characterised DMD
425 phenotypes including muscle features and metabolism dysregulations as well as fibrosis. Altogether, these
426 data argue for 1) a deficit and not a delay in DMD differentiation; 2) seeing DMD as a progressive
427 developmental disease as well as a metabolic pathology whose onset is triggered before the entry into the
428 skeletal muscle compartment; and 3) fibrosis as an intrinsic feature of DMD muscle cells. Future studies could
429 explore the additional roles of *DMD* locus products and the impact of their loss during skeletal muscle
430 development, as well as find earlier and more specific disease biomarkers and develop combination
431 therapeutic strategies using high-throughput drug screening.

432 All the omics data from this study will be soon available online for exploration through a graphical interface.
433 For additional information, please send an email to shiny@virginie-mournetas.fr.

434 **MATERIALS AND METHODS**

435 **Ethics, consent, and permissions**

436 At the Cochin Hospital-Cochin Institute, the collection of primary cultures of myoblasts was established from
437 patient muscle biopsies conducted as part of medical diagnostic procedure of neuromuscular disorders. For
438 each patient included in this study, signed informed consent was obtained to collect and study biological
439 resources, and establish primary cultures of fibroblasts and myoblasts at the Hospital Cell Bank-Cochin
440 Assistance Publique—Hôpitaux de Paris (APHP). This collection of myoblasts was declared to legal and ethical
441 authorities at the Ministry of Research (number of declaration, 701, n° of the modified declaration, 701–1) via
442 the medical hosting institution, APHP, and to the “Commission Nationale de l’Informatique et des Libertés”
443 (CNIL, number of declaration, 1154515).

bioRxiv preprint doi: https://doi.org/10.1101/720920. The copyright holder for this preprint (which was not peer-reviewed) is the author/funder. It is made available under a CC-BY-NC 4.0 International license.

444 **Cells**

445 Human primary adult myoblasts from healthy individuals and DMD patients were provided by Celogos and
446 Cochin Hospital-Cochin Institute (Table S3). In Celogos laboratory, cell preparation was done according to
447 patent US2010/018873 A1.

448 **Cell culture**

449 ***Human tissue-derived myoblasts –*** Primary myoblasts were maintained in a myoblast medium: DMEM/F-12,
450 HEPES (31330–038, Thermo Fisher Scientific) supplemented with 10 % fetal bovine serum (FBS, Hyclone,
451 Logan, UT), 10 ng/mL fibroblast growth factor 2 (FGF2, 100-18B, Peprotech), and 50 nM Dexamethasone
452 (D4902, Sigma-Aldrich) on 0.1 % gelatin (G1393, Sigma-Aldrich) coated culture ware.

453 ***Human tissue-derived myotubes –*** Primary myoblasts were differentiated into myotubes. Cells were seeded at
454 600 cells/cm^2 on 0.1 % gelatin coated cultureware in myoblast medium containing 1 mM Acid ascorbic 2P
455 (A8960, Sigma-Aldrich).

456 ***Human induced pluripotent stem cells –*** Primary myoblasts were reprogrammed into hiPSCs following the
457 protocol described in (15), using the Yamanaka's factors POU5F1, SOX2 and KLF4 transduction by ecotropic or
458 amphotropic vectors (Table S3). HiPSCs were adapted and maintained with mTeSR™1 culture medium (05850,
459 Stemcell Technologies) on Corning® Matrigel® Basement Membrane Matrix, lactose dehydrogenase elevating
460 virus (LDEV)-Free-coated cultureware (354234, Corning Incorporated). Cells were then seeded at 20,000
461 cells/cm^2, passaged and thawed each time with 10 µM StemMACS™ Y27632.

462 ***Human iPSC-derived cell –*** *S*ix hiPSCs (3 healthy and 3 DMD) were differentiated three times toward skeletal
463 muscle lineage using commercial media designed from Caron's work (23) (Skeletal Muscle Induction
464 medium SKM01, Myoblast Cell Culture Medium SKM02, Myotube Cell Culture Medium SKM03, AMSbio). This
465 protocol is a 2D directed differentiation that uses 3 consecutive defined media (SKM01 from day 0 to 10,
466 SKM02 from day 10 to 17 and SKM03 from day 17 to d25) and only one cell passage at day 10. Cells were
467 seeded at 3,500 cells/cm^2 at day 0 and day 10 on BioCoat™ Collagen I cultureware (356485, Corning
468 Incorporated). Part of the cell culture was frozen at day 17 for further experiments such as DNA extraction.

bioRxiv preprint doi: https://doi.org/10.1101/720920. The copyright holder for this preprint (which was not peer-reviewed) is the author/funder. It is made available under a CC-BY-NC 4.0 International license.

469 These cells were then thaw at 30,000 cells/cm^2, and cultured in SKM02 for 3 days and SKM03 for 3 additional
470 days to get myotubes.

471 **DNA and RNA experiments**

472 ***RNA extraction and quality –*** RNA extraction was done in the six cell lines at 7 different time points: tissue-
473 derived myoblast and tissue-derived myotube, as well as during hiPSC differentiation at day 0, 3, 10, 17 and 25
474 (hiPSC-derived myotube) using the miRNeasy Mini kit (217004, QIAgen) on the QIAcube instrument. RNAs
475 coming from the part A of the extraction protocol was used for mRNA-seq and RT-qPCR. RNAs coming from the
476 part B of the extraction protocol was used for miRseq. PartA RNA was quantified on Nanodrop
477 spectrophotometer (ND-1000, Thermo Fisher Scientific) and purity/quality (RIN ≥ 7) was assessed on the 2200
478 TapeStation using the Agilent RNA ScreenTape (5067-5576 / 5067-5577 / 5067-5578, Agilent). PartB RNA was
479 quantified and purity/quality was assessed on the 2100 Agilent BioAnlayzer using the Agilent small RNA kit
480 (5067-1548, Agilent).

481 ***Reverse transcription –*** 500 ng of total RNA were reverse transcribed with random primers (48190–011,
482 Thermo Fisher Scientific), oligo(dT) (SO131, Thermo Fisher Scientific), and deoxynucleotide (dNTP, 10297–018,
483 Thermo Fisher Scientific) using Superscript® III reverse transcriptase (18080–044, Thermo Fisher Scientific).
484 Thermocycling conditions were 10 min, 25 °C; 60 min, 55 °C; and 15 min, 75 °C.

485 ***qPCR –*** We amplified cDNA/total DNA using primers (Thermo Fisher Scientific) listed in Table S6. They were
486 designed using Primer blast (http://www.ncbi.nlm.nih.gov/tools/primer-blast). The amplification efficiency of
487 each primer set was preliminarily determined by running a standard curve. Detection was performed using a
488 QuantStudio™ 12K Flex Real-Time PCR System (Thermo Fisher Scientific). Reactions were carried out in a 384-
489 well plate, with 10 µL containing 2.5 µL of 1/10 cDNA or 6.25 ng/uL total DNA, 0.2 µL of mixed forward and
490 reverse primers at 10 µM each, and 5 µL of 2X Luminaris Color HiGreen qPCR Master Mix Low Rox (K0973,
491 Thermo Fisher Scientific). Thermocycling conditions were 50 °C during 2 min, 95 °C during 10 min, followed by
492 45 cycles including 15 sec at 95 °C, 1 min at 60 °C plus a dissociation stage. All samples were measured in
493 triplicate. Experiments were normalised using UBC as reference gene and relative quantification was done
494 with the ΔΔCt method.

bioRxiv preprint doi: https://doi.org/10.1101/720920. The copyright holder for this preprint (which was not peer-reviewed) is the author/funder. It is made available under a CC-BY-NC 4.0 International license.

495 ***mRNA-seq*** **–** Libraries are prepared with TruSeq Stranded mRNA kit protocol according supplier
496 recommendations. Briefly, the key stages of this protocol are successively, the purification of PolyA containing
497 mRNA molecules using poly-T oligo attached magnetic beads from 1µg total RNA, a fragmentation using
498 divalent cations under elevated temperature to obtain approximately 300bp pieces, double strand cDNA
499 synthesis and finally Illumina adapter ligation and cDNA library amplification by PCR for sequencing.
500 Sequencing is then carried out on paired-end 100 b/75 b of Illumina HiSeq 4000.
501 An RNA-seq analysis workflow was designed using snakemake 3.5.4 (153) for read quality estimation, mapping
502 and differential expression analysis. Quality estimation was obtained with FastQC 0.11.5
503 (https://www.bioinformatics.babraham.ac.uk/projects/fastqc/). Mapping to the human genome assembly
504 Ensembl GRCh37.87 (43,695 transcripts) was performed with STAR 2.5.0a (154). According to STAR manual and
505 for more sensitive novel junction discovery, the junctions detected in a first round of mapping were used in a
506 second mapping round. Read strandness was confirmed using RSeQC (155). Analysis results were summarised
507 using MultiQC 1.0 (156). Normalised counts (median ratio normalisation, MRN) and differential expression
508 analysis was performed with DESeq2 1.16.1 (157), considering pairwise comparisons with all developmental
509 stages and comparing DMD versus healthy cells within developmental stages. BiomaRt 2.30.0 (158) was used
510 to fetch gene annotations from Ensembl. Transcripts with |log2FoldChange| ≥ 0.4 (equivalent of DMD/healthy
511 ratio ≤ 0.76 or ≥ 1.32) and adjusted p-value ≤ 0.05 were considered differentially expressed. RNA-seq data
512 have been deposited in the ArrayExpress database (159) at EMBL-EBI under accession number E-MTAB-8321
513 (https://www.ebi.ac.uk/arrayexpress/experiments/E-MTAB-8321).

514 ***miRNA-seq*** **–** 10 ng of miRNA was reverse transcribed using the Ion Total RNA-seq kit v2
515 (4475936, Thermofisher Scientific) following the protocol of the manufacturer for small RNA libraries. The
516 cDNA libraries were amplified and barcoded using Ion Total RNA-seq kit v2 and Ion Xpress RNA-seq Barcode
517 Adapters 1-16 Kit (Thermofisher Scientific). The amplicons were quantified using Agilent High Sensitivity DNA
518 kit before the samples were pooled in sets of fifteen. Emulsion PCR and enrichment was performed on the Ion
519 OT2 system Instrument using the Ion PI Hi-Q OT2 200 kit (A26434, Thermofisher Scientific). Samples were
520 loaded on an Ion PI v3 Chip and sequenced on the Ion Proton System using Ion PI Hi-Q sequencing 200 kit
521 chemistry (200 bp read length; A26433, Thermofisher Scientific). Sequencing reads were trimmed with Prinseq
522 (160) (v0.20.4) (--trim-right 20) and filtered by average quality score (--trim-qual 20). Reads with a size less

bioRxiv preprint doi: https://doi.org/10.1101/720920. The copyright holder for this preprint (which was not peer-reviewed) is the author/funder. It is made available under a CC-BY-NC 4.0 International license.

523 than 15 bp have been removed and reads with a size greater than 100 bp have been trimmed with Cutadapt
524 (v1.16)(161). Mapping to the human genome assembly Ensembl GRCh37.87 (3111 transcripts) was performed
525 with STAR 2.5.3a (154). Normalised counts (median ratio normalisation, MRN) and differential expression
526 analysis was performed with DESeq2 1.16.1 (157), considering pairwise comparisons with all developmental
527 stages and comparing DMD versus healthy cells within developmental stages. Transcripts with
528 |log2FoldChange| ≥ 0.4 (equivalent of DMD/healthy ratio ≤ 0.76 or ≥ 1.32) and p-value ≤ 0.05 were considered
529 differentially expressed. The use of p-value instead of adjusted p-value is justified by biological meaning(162)
530 (i.e. well-known regulated / dysregulated miRNAs had a p-value ≤ 0.05 but not an adjusted p-value ≤ 0.05).
531 miRNA-seq data have been deposited in the ArrayExpress database (159) at EMBL-EBI under accession number
532 E-MTAB-8293 (https://www.ebi.ac.uk/arrayexpress/experiments/E-MTAB-8293).

533 ***High-throughput data analyses –*** Graphs were realised using RStudio. Viridis 0.5.1 library (163) was used for
534 the colour palette easier to read with colour blindness and print well in grey scale. For unsupervised analyses,
535 normalised counts were standardised with scale function (center = TRUE, scale = TRUE) and plotted with
536 corrplot function from corrplot 0.84 library (164). Spearman correlation was done with the cor function
537 (method = "spearman", use = "pairwise.complete.obs") on standardised data. Hierarchical clustering and
538 heatmap were performed with gplots 3.0.3 library (165) heatmap.2 function on standardised data. Gene
539 enrichment data were retrieved from DAVID database using RDAVIDWebService 1.24.0 library (166) on
540 supervised list of mRNAs (mRNA-seq data: adjusted p-value ≤ 0.01, normalised counts ≥ 5 in at least one
541 sample, ratio ≤ 0.5 or ≥ 2 for myogenesis (Figure S2B) and ratio ≤ 0.76 or ≥ 1.32 for DMD phenotype (Figure
542 S2C); enrichment data: Benjamini value ≤ 0.05, enrichment ≥ 1.5). Only Gene Ontology terms were processed.
543 Spearman correlations for the comparison transcriptomics vs proteomics at day 17 and for comparisons with
544 published omics datasets were performed using two-tailed nonparametric Spearman correlation on GraphPad
545 Prism software.

546 ***Exon skipping –*** 1,000,000 healthy M180 cells were transfected after 17 days of culture by electroporation
547 with a phosphorodiamidate morpholino oligo (PMO) targeting exon 7 of the *DMD* gene at 10 or 100 µM, or a
548 PMO Control at 100 µM in 100 µL solution from the P3 Primary Cell 4D-Nucleofector® X Kit L (V4XP-3024,
549 Lonza) using the CB150 program on the 4D-Nucleofector™ System (Lonza). Cells were seeded at a density of
550 100,000 cells/cm². RNA extraction was carried on transfected cells 24 h, 48 h and 72 h later followed by RT as

bioRxiv preprint doi: https://doi.org/10.1101/720920. The copyright holder for this preprint (which was not peer-reviewed) is the author/funder. It is made available under a CC-BY-NC 4.0 International license.

551 described above. PCR was done on1 uL of cDNA using 10 µM of forward and reverse primers (Fw 5'-
552 AAGATTCTCCTGAGCTGGGTC -3' and Rv 5'- AGTCACTTTAGGTGGCCTTGG -3', Life technologies) and 1 U Taq
553 DNA polymerase (10342, Life technologies) as described by the manufacturer's instructions, for a final reaction
554 volume of 25 µL. PCR reaction started by a step at 94°C for 3 min, followed by 27 cycles at 94°C for 45 s, 55°C
555 for 45 s and 72°C for 45 s, and a final step at 72°C for 5 min. Exon skipping was analyzed using the DNA 1000 kit
556 (5067, Agilent) on the Agilent 2100 Bioanalyzer. Full length PCR product was 372 bp and exon skipped length
557 PCR product was 253 bp. Results were computed by the Agilent 2100 Bioanalyzer software v3.81. Spearman
558 correlations were performed using two-tailed nonparametric Spearman correlation on GraphPad Prism
559 software.

560 **Protein experiments**

561 ***Immunolabelling* –** Cells (healthy hiPSC 1/ DMD hiPSC 2, Table S5) at day 17 of culture were thawed and
562 seeded at 10,000 cells/cm^2 in SKM02 medium in Falcon® 96-well microplate (353219, Corning) coated with
563 0.1% gelatin (G1393, Sigma-Aldrich) and 2.4 µg/mL laminin (23017015, Thermofischer Scientific) in PBS 1X
564 (D8537, Sigma-Aldrich). After 4 days, cells were switched to DMEM/F-12, HEPES (31330038, Thermofischer
565 Scientific) with 2% Horse serum (H1270, Sigma-Aldrich). Before staining, after removing the culture medium,
566 cells were fixed 15 min at 4°C with PFA 4% (15710, Euromedex) after 7 days of culture. A first quick Phosphate
567 buffered saline (PBS) 1X tablets (P4417, Sigma-Aldrich) wash was done, followed by another lasting 10 min.
568 Then, a solution with PBS 1X, Triton™ X-100 0.25% (T8787, Sigma-Aldrich) and Bovine serum albumin 2.5%
569 (BSA, A9418, Sigma-Aldrich) was added and incubated 30 min at room temperature. Primary antibody was
570 finally added, diluted in the same buffer (α-actinin 1/500, A7811, Sigma-Aldrich), overnight at 4°C. The next
571 day, two quick PBS 1X washes were followed by a third incubated 10 min at room temperature. An incubation
572 was done 45 min at room temperature with a mix of 4′,6-Diamidine-2′-phenylindole dihydrochloride (DAPI,
573 1µg/mL, 10236276001, Sigma-Aldrich) and the secondary antibody Donkey anti-Mouse Alexa Fluor 555 in PBS
574 1X, (1/1000, A-31570, Thermofischer Scientific). Finally, two quick PBS 1X washes were followed by a third
575 incubated 10 min at room temperature. The stained cells were kept in PBS 1X at 4°C before imaging with a
576 Zeiss LSM880 Airyscan confocal and Zen software (Black edition).

bioRxiv preprint doi: https://doi.org/10.1101/720920. The copyright holder for this preprint (which was not peer-reviewed) is the author/funder. It is made available under a CC-BY-NC 4.0 International license.

577 ***Western blotting*** **–** For tissue-derived myotubes, after three rinses with cold PBS 1X (w/o Ca2+ and Mg2+,
578 D8537, Sigma-Aldrich), protein extracts were isolated from cultured cells by scraping (010154, Dutscher) with
579 an extraction protein buffer (NaCl 150 mM, Tris 50 mM, EDTA 10 mM (AM9260G, ThermoFisher Scientific),
580 Triton 1X, 1/100 Protease Inhibitor Cocktail (P8340, Sigma-Aldrich), PhosSTOP tablet (04906845001, Roche
581 Diagnostics)). For hiPSC-derived myotubes, cell pellets were rinsed once with cold PBS 1X, spun 5 min at 300 g
582 and resuspended in the same extraction protein buffer. Protein Extracts were centrifuged at 4°C 10 min at
583 16,000 g and supernatants were kept at −80 °C. Quantitation of total protein was done with Pierce BCA protein
584 assay kit (23225, ThermoFischer Scientific). Before gel loading, protein extracts were mixed with 9µL of loading
585 buffer (Urea 4M, SDS 3.8%, Glycerol 20%, Tris 75mM pH 6.8, 5% β-mercaptoethanol, 0.1mg/mL Bromophenol
586 blue) and completed to 28µL (for one well) with extraction protein buffer, then heated once 5 min at 95 °C.
587 Western blots were performed either with Criterion ™ XT Tris-Acetate Precast Gels 3–8 % (3450130, Bio-Rad,
588 Hercules, CA), XT Tricine running buffer (161–0790, Bio-Rad) and ran at room temperature for 1 hour and 15
589 min at 150 V for RYR1 (1/1000, MA3-925, ThermoFisher Scientific), MF20 (1/500, DSHB, concentrate),
590 Manex50 (1/30, DSHB), α-sarcoglycane (1/150, A-SARC-L-CE, Leica biosystems), γ-sarcoglycane (1/150, G-
591 SARC-CE, Leica biosystems), or with 4–15% Criterion™ TGX™ Precast Midi Protein Gel (5671084, Bio-Rad), 10x
592 Tris/Glycine/SDS Running Buffer (1610772), and ran at room temperature for 1 hour at 200 V for CaV1.1
593 (1/1000, MA3-920, ThermoFisher Scientific), ATP5A (1/1,000, ab14748, ABCAM), Semaphorin 6A (1/55,
594 AF1146, R&D systems) and GLI3 (1/200, AF3690, R&D systems). Gels were rinsed once in water and blotted
595 either with "high molecular weight" or "mixed molecular weight" program of TransBlot® Turbo™ transfer
596 system (Bio-Rad) using Trans-Blot®Turbo™ Midi Nitrocellulose Transfer Packs (170–4159, Bio-Rad). Blots were
597 then processed with the SNAP i.d.® 2.0 Protein Detection System following the manufacturer's protocol, with
598 Odyssey® Blocking Buffer (927-40003, LI-COR) for blocking and with 0,2% Tween® 20 added for antibody
599 dilutions (28829.296, VWR), washes were done with phosphate-buffered saline tween (PBST) buffer (PBS 1X
600 tablets, P4417, Sigma-Aldrich; 0.1 % Tween® 20). Every primary antibody was pooled with either α-actinin
601 (1/12,500, sc-17829, Santa Cruz or 1/7000, A7811, Sigma-Aldrich) or α-tubulin (1/6666, Ab7291, Abcam). For
602 secondary antibodies, either IRDye 800CW donkey anti-mouse and/or IRDye® 680RD donkey anti-goat were
603 used (1/5000-1/10000, 926-32212, 926-68074, LI-COR). After completion of SNAP i.d.® general protocol, with
604 the membrane still in the blot holder, two PBS 1X washes were finally done before band visualisations with

bioRxiv preprint doi: https://doi.org/10.1101/720920. The copyright holder for this preprint (which was not peer-reviewed) is the author/funder. It is made available under a CC-BY-NC 4.0 International license.

605 Odyssey® CLx Imaging System and quantification with Image Studio Lite software (Version 5.2). Statistical
606 analysis was performed using unpaired t test on GraphPad Prism software.

607 ***TMT Isobaric quantitative proteomics –***

608 *Samples Preparation:* Cells at day 17 were collected and resuspended in 90% FBS (Hyclone), 10% DMSO
609 (A3672.0050, VWR), cooled down until -90°C with the CryoMed™ device (ThermoFisher Scientific), before
610 storage in liquid nitrogen. Cells were then thawed and washed 5 times with cold PBS and air was replaced by
611 Argon to thoroughly dry the pellet that was flash frozen in liquid nitrogen. 5-10 times the approximate cell
612 pellet volume of 0.5 M triethyl ammonium bicarbonate (TEAB) with 0.05% SDS was added to the cell pellet for
613 protein extraction. Cell pellet was re-suspended and triturated by passing through a 23-gauge needle and 1ml
614 syringe for 30 times. Samples were then sonicated on ice at amplitude of 20% for 30 x 2 sec bursts and
615 centrifuged at 16000g for 10 min at 4°C. Supernatant was transferred to a fresh Eppendorf tube. Protein was
616 quantified by nanodrop. 100-150µg of protein was aliquoted for each individual sample and 2µl TCEP (50mM
617 tris-2-carboxymethyl phosphine) was added for every 20µl of protein used for reducing the samples. After 1 hr
618 incubation at 60°C, 1µl MMTS (200mM methylmethane thiosulphonate) was added for every 20µl of protein
619 used for alkylating/'blocking' the samples. Finally, after a 10 min incubation at RT, samples were trypsinised by
620 addition of 6-7.5µl of 500ng/µl trypsin. The ration between enzyme: substrate was 1:40. Samples were
621 incubated overnight at 37°C in the dark. *TMT labelling:* When TMT reagents reached room temperature, 50µl
622 of isopropanol/[acetonitrile] was added to each TMT 11-plex reagent and was incubated at RT for 2 hrs, in the
623 dark. 8 µl of 5% hydroxylamine was added to neutralise the reaction. Each sample was separately lyophilised
624 at 45°C. Samples have been stored at -20°C or used immediately.

625 *Offline C4 High Performance Liquid Chromatography (HPLC):* All 8 samples were pooled together in 60µl of 97%
626 mobile phase A (99.92% % H2O, 0.08% NH_4OH) and 3% mobile phase B (99.92% % Acetonitrile, 0.02% NH_4OH)
627 by serially reconstituting each sample. Extra 40µl of mobile phase was added to sample 1, after sample has
628 been well vortexed, all the contents of sample 1 tube were transferred to the tube with the sample 2 (and
629 serially repeated until all samples were pooled). Final volume of samples needed to be 100µl. After sample was
630 centrifuged at 13000g for 10 min, supernatant was collected with an HPLC injection syringe. 100µl was injected
631 onto the sample loop. Fractions were collected in a peak dependent manner. Finally, fractions were lyophilised
632 at 45°C and stored at -20°C until required. The used column was a Kromasil C4 column 100Å pore size, 3.5µm

bioRxiv preprint doi: https://doi.org/10.1101/720920. The copyright holder for this preprint (which was not peer-reviewed) is the author/funder. It is made available under a CC-BY-NC 4.0 International license.

633 particle size, 2.1mm inner diameter and 150mm length. The gradient for C4 separation was (RT in min - %B): 0-
634 3; 10-3; 11-5; 16-5; 65-20; 100-30; 15-80; 120-80; 125-3.

635 *Solid Phase Extraction Cleaning of peptides fractions:* A GracePureTMT SPE C18-Aq cartridge was used for pre-
636 cleaning of samples (Support: Silica, % Carbon: 12.5%, With endcapping, Surface area: 518m^2/g, Particle size:
637 50μm, Pore size: 60Å, Water-wettable). Samples were reconstituted using in total 400μl of 1% ACN, 0.01% FA.
638 Cartridge was washed with 600μl of ACN. ACN was then completely flushed out of the column at dropwise
639 speed. This activated the ligands. Then 1% ACN, 0.01% FA (600μl) was flushed through the cartridge to
640 equilibrate the sorbent. 400μl of the sample was loaded in the cartridge. It was then very slowly flushed
641 through the cartridge and recovered into a fresh tube. This process was repeated 3 times. 2 volumes of 250μl
642 of 1%ACN, 0.01%FA were used to clean and de-salt the sample. It was flushed through very slowly. 2 volumes
643 (250μl each) were used per step (2% ACN, 10% ACN, 30% ACN, 50% ACN, 70% ACN). This cycle was repeated
644 twice. Each particular concentration was pooled in one tube. Samples were dried to dryness in a Speedvac at
645 RT overnight and stored at -20°C. Like previously, samples were pooled with 100μl of 97% mobile phase A
646 (99.92% % H2O, 0.08% NH_4OH) and 3% mobile phase B (99.92% % Acetonitrile, 0.02% NH_4OH) and injected
647 onto the sample loop. Fractions were collected in a peak dependent manner. The gradient for SPE cleaned
648 peptides C4 separation (RT in min - %B): 0-2; 10-2; 20-5; 25-5; 35-20; 55-35; 60-35; 70-80; 75-80; 80-3.

649 *Online C18 High Precision Liquid Chromatography (HPLC):* 30μl of loading phase (2% acetonitrile, 1.0% formic
650 acid) was added to each fraction-containing Eppendorf tube. Samples were vortexed and centrifuged. Blanks
651 (30μl mobile phase) were added into well A1 to A12. 30μl of sample 1 was pipetted into well B1, sample 2 in
652 well B2 and so on. An orthogonal 2D-LC-MS/MS analysis was performed with the Dionex Ultimate 3000 UHPLC
653 system coupled with the ultra-high-resolution nano ESI LTQ-Velos Pro Orbitrap Elite mass spectrometer
654 (Thermo Scientific).

655 *Data analysis:* HCD and CID tandem mass spectra were collected and submitted to Sequest search engine
656 implemented on the Proteome Discoverer software version 1.4 for peptide and protein identifications. All
657 spectra were searched against the UniProtKB SwissProt. The level of confidence for peptide identifications was
658 estimated using the Percolator node with decoy database searching. False discovery rate (FDR) was set to 0.05,
659 and validation was based on the q-Value. Protein ratios were normalised to protein median and peptides with
660 missing TMT values were rejected from protein quantification. Phosphorylation localisation probability was
661 estimated with the phosphoRS node. Protein ratios were transformed to log_2 ratios and significant changes

bioRxiv preprint doi: https://doi.org/10.1101/720920. The copyright holder for this preprint (which was not peer-reviewed) is the author/funder. It is made available under a CC-BY-NC 4.0 International license.

662 were determined by one sample T-test. To reduce the impact of possible false positive identifications, more
663 parameters were set: 1) only proteins with more than two quantified unique peptides. 2) DMD/Healthy ratio ≥
664 1.32 or ≤ 0.76 and 3) only FDR corrected p-value ≤ 0.05 were retained for bioinformatics analysis. The list of
665 proteins quantified in the 6 samples is in Table S3. Proteomic data have been deposited in the PRIDE Archive
666 database (167) at EMBL-EBI under accession number PXD015355
667 (https://www.ebi.ac.uk/pride/archive/projects/PXD015355).

668 **ATP experiments** – Two healthy (M180 and M398) and two DMD (M202 and M418) cell lines after 17 days of
669 culture were seeded in 384-well plates at a density of 30,000 cells/cm^2. Living cells were staining with
670 HOECHST at a concentration of 1/300 six days later for cell quantification (nuclei per well were counted using
671 the CX7 imaging system, ThermoFisher). ATP measure was done using the CellTiter-Glo™ Luminescent Cell
672 Viability Assay Kit (Promega) following the manufacturer's protocol and normalised by the cell quantification.
673 Statistical analysis was performed using one-sample t test on GraphPad Prism software (each healthy cell line
674 was compared to each DMD cell line).

675 **COMPETING INTERESTS**

676 The authors declare that they have no competing interests.

677 **FUNDING**

678 We thank the Fondation Maladies Rares (GenOmics grant), Labex Revive (Investissement d'Avenir; ANR-10-
679 LABX-73) and the AFM Téléthon for funding this project.

680 **ACKNOWLEDGEMENTS**

681 The RNA-Sequencing libraries were processed and sequenced by Integragen (Evry, France). We gratefully
682 acknowledge support from the PSMN (Pôle Scientifique de Modélisation Numérique) of the ENS de Lyon for
683 the computing resources. We thank Dr Nacira Tabti, Dr Elisabeth Le Rumeur, Dr Nathalie Deburgrave and Dr
684 Malgorzata Rak for providing us with specific reagents and antibodies. We thank Dr Linda Popplewell for

bioRxiv preprint doi: https://doi.org/10.1101/720920. The copyright holder for this preprint (which was not peer-reviewed) is the author/funder. It is made available under a CC-BY-NC 4.0 International license.

685 designing and validating the PMO7 sequence. We thank Dr David Israeli for his feedback on the manuscript
686 and overall discussion on our project.

bioRxiv preprint doi: https://doi.org/10.1101/720920. The copyright holder for this preprint (which was not peer-reviewed) is the author/funder. It is made available under a CC-BY-NC 4.0 International license.

687 **FIGURE LEGENDS**

688 **Figure 1 – Differentiation dynamics of hiPSCs (D0) into MyoT (D25) in healthy cells at the transcriptomic**
689 **level. A)** Spearman correlation matrix of transcriptomes (mRNAs, right) and miRnomes (miRNAs, left). Yellow
690 dots indicate a stronger correlation. **B)** Gene expression heatmap of selected differentiation markers. (D: day;
691 hiPSC: human induced pluripotent stem cell; MyoT: myotube).

692 **Figure 2 – Differentiation dynamics of hiPSCs (D0) into MyoT (D25) in DMD cells. A)** Dotplot of DMD/healthy
693 expression ratios of selected differentiation markers. Statistical differences are indicated in brackets after gene
694 names, and grey circles around the corresponding dots. **B)** Proportions of significantly dysregulated mRNAs
695 (adjusted p-value ≤ 0.05) in DMD cells at each time points. Expression of **C)** *MIR1-1* and **D)** *ATP2A2* mRNA
696 during differentiation. **E)** ATP2A2 protein level at D17. (*adjusted p-value ≤ 0.05, **adjusted p-value ≤ 0.01,
697 ***adjusted p-value ≤ 0.001, ****adjusted p-value ≤ 0.0001; D: day; hiPSC: human induced pluripotent stem
698 cell; MyoT: myotube).

699 **Figure 3 – Comparison of healthy and DMD MyoT from hiPSCs and tissues at the protein level. A)** hiPSC-
700 derived MyoT immunolabelling of α-actinin (red) and nuclei (DAPI, blue) in healthy (left) and DMD cells (right).
701 **B)** Representative Western blots and related quantifications of DMD, SGCA, SGCG, myosin heavy chains,
702 CACNA1S and RYR1 from protein extracts in healthy and DMD hiPSC-derived and tissue-derived MyoT (X: 0.25
703 µg of total protein was used in hiPSC-derived MyoT instead of 7µg in tissue-derived MyoT - *p-value ≤ 0.05,
704 **p-value ≤ 0.01, ***p-value ≤ 0.001, ****p-value ≤ 0.0001). (hiPSC: human induced pluripotent stem cell;
705 MyoT: myotube).

706 **Figure 4 – Manifestation of the DMD phenotype in the transcriptome and miRnome of myotubes derived**
707 **from hiPSCs and tissues. A)** Hierarchical clustering and heatmap in healthy hiPSCs (D0), hiPSC-derived MyoT
708 and tissue-derived MyoT with selected skeletal muscle transcripts and miRNAs. **B)** Volcano plots of
709 dysregulated mRNAs/miRNAs in hiPSC-derived MyoT (left) and tissue-derived MyoT (right) – vertical grey
710 dashed lines represent DMD/Healthy ratio thresholds at 0.76 or 1.32 - the horizontal grey dashed line
711 represents the adjusted p-value threshold at 0.05. Comparisons of DMD/Healthy expression ratios at D17 and
712 D25 with published omics data from muscle biopsies (4,97) : **C)** number of genes in black and Spearman
713 correlation coefficients in brown found in common with Pescatori *et al.*'s mRNA data (top) and Capitanio *et*

bioRxiv preprint doi: https://doi.org/10.1101/720920. The copyright holder for this preprint (which was not peer-reviewed) is the author/funder. It is made available under a CC-BY-NC 4.0 International license.

714 *al.*'s protein data (bottom) as well as **D)** correlation graphs of the D25 data compared with Pescatori *et al.*
715 mRNA data (left) and Capitanio *et al.* protein data (right). Genes with |log2FoldChange| ≥ 0.4 are in blue if
716 adjusted p-value ≥ 0.05 and yellow if adjusted p-value ≤ 0.05. (DAPC: dystrophin-associated protein complex;
717 hiPSC: human induced pluripotent stem cell; MyoT: myotube; NMJ: neuromuscular junction; TF: transcription
718 factor MyoT - *p-value ≤ 0.05, **p-value ≤ 0.01, ***p-value ≤ 0.001, ****p-value ≤ 0.0001).

719 **Figure 5 – Illustration of the fibrosis phenotypes in DMD cells.** Volcano plots of dysregulated mRNAs/miRNAs
720 related to **A)** the SHH pathway and collagen metabolism at D10/17/25; and **B)** fibrosis at D25 – vertical grey
721 dashed lines represent DMD/Healthy ratio thresholds at 0.76 or 1.32 - the horizontal grey dashed line
722 represents the adjusted p-value threshold at 0.05. (D: day; MMP: matrix metallopeptidase; SHH: sonic
723 hedgehog pathway; TIMP: tissue inhibitor of metallopeptidase; TGF: transforming growth factor).

724 **Figure 6 – Illustration of the metabolic and mitochondrial phenotypes in DMD cells.** Volcano plots of
725 dysregulated mRNAs/miRNAs related to **A)** principal metabolic pathways; and **B)** the constitution of the five
726 mitochondrial respiratory complexes in DMD hiPSC-derived MyoT – vertical grey dashed lines represent
727 DMD/Healthy ratio thresholds at 0.76 or 1.32 - the horizontal grey dashed line represents the adjusted p-value
728 threshold at 0.05. Quantification of ATP5A1 expression **C)** at the mRNA level during differentiation, and **D)** at
729 the protein level at D17 (TMT proteomic data, left) and D25 (Western blot data, right). **E)** Measure of ATP
730 levels in DMD cell lines, relative to Healthy controls. (*adjusted p-value ≤ 0.05, **adjusted p-value ≤ 0.01,
731 ***adjusted p-value ≤ 0.001, ****adjusted p-value ≤ 0.0001). (D: day; hiPSC: human induced pluripotent stem
732 cell, MyoT: myotube)

733 **Figure 7 – Mitochondrial dysregulations in DMD cells during differentiation. A)** Absolute (top) and relative
734 numbers (%, bottom) of dysregulated genes from the different mitochondrial compartments over the course
735 of DMD hiPSC differentiation. **B)** Expression ratios of selected mitochondrial proteins. Statistical differences
736 are indicated in brackets (*adjusted p-value ≤ 0.05, **adjusted p-value ≤ 0.01, ***adjusted p-value ≤ 0.001,
737 ****adjusted p-value ≤ 0.0001). **C)** Volcano plots of mitochondria-related genes over the course of DMD hiPSC
738 differentiation. Statistical differences are symbolised with orange dots – vertical grey dashed lines represent
739 DMD/Healthy ratio thresholds at 0.76 or 1.32 - the horizontal grey dashed line represents the adjusted p-value

bioRxiv preprint doi: https://doi.org/10.1101/720920. The copyright holder for this preprint (which was not peer-reviewed) is the author/funder. It is made available under a CC-BY-NC 4.0 International license.

740 threshold at 0.05 – The percentage of significantly dysregulated genes is indicated at the bottom right in grey.
741 (D: day).

742 **Figure S1 – DMD variant expression over the course of hiPSC differentiation. A)** Bright field microscope
743 pictures at the 7 differentiation points giving rise to hiPSC-derived and tissue-derived MyoT. Possible
744 cryopreservation time points are indicated by snowflakes. **B)** RT-qPCR relative quantification of *DMD* variants
745 expression during differentiation of hiPSCs (D0) into MyoT (D25) with the related cycle threshold (CT) values
746 (Ct: cycle threshold; D: day; hiPSC: human induced pluripotent stem cell; MyoB: myoblast; MyoT: myotube).

747 **Figure S2 – Gene ontology enrichments over the course of healthy and DMD hiPSC differentiation A)**
748 Proportions of significantly regulated mRNAs (adjusted p-value ≤ 0.01) between successive differentiation time
749 points during the differentiation of healthy hiPSCs. Gene ontology enrichments on **B)** significantly regulated
750 mRNAs between successive differentiation time points in healthy cells (number of genes in brackets) and **C)**
751 significantly dysregulated mRNAs at each differentiation time points in DMD cells. The number of genes
752 involved in these significant enrichments is indicated in brackets next to each GO term. In green, GO terms
753 related to downregulated genes and in yellow, GO terms related to upregulated genes (BP: biological process;
754 CC: cellular component; D: day; hiPSC: human induced pluripotent stem cell; MyoB: myoblast; MyoT:
755 myotube).

756 **Figure S3 – Comparison of healthy and DMD cells at D10 and D17, protein analyses.** Western blots and
757 quantifications of **A)** SEMA6A at D10, **B)** GLI3 at D10 and **C)** GLI3 at D17. Omics comparison of mRNA and
758 protein data at day 17: **D)** Venn diagram of the number of genes with |log2FoldChange| ≥ 0.4 and adjusted
759 pvalue ≤ 0.05 in either transcriptomic or proteomic data, **E)** their associated Spearman correlation coefficient
760 in brown, as well as **D)** their correlation graph with the number of genes with |log2FoldChange| ≥ 0.4 in both
761 sets are indicated (genes with p-value ≥ 0.05 only in transcriptomics are in blue, only in proteomics in purple
762 and in both in orange). (*p-value ≤ 0.05, **p-value ≤ 0.01, ***p-value ≤ 0.001, ****p-value ≤ 0.0001; D: day;
763 GLI3FL: GLI3 full length; GLI3R: GLI3 repressor).

764 **Figure S4 – *DMD* knockdown at D17 in healthy cells. A)** qPCR quantification of *DMD* expression related to
765 exon skipping efficiency (%); **B)** Western blot quantification of dystrophin; and **C)** qPCR quantification of
766 selected genes following exon skipping (boxplots of expression ratio of exon 7 skipped/unskipped conditions

bioRxiv preprint doi: https://doi.org/10.1101/720920. The copyright holder for this preprint (which was not peer-reviewed) is the author/funder. It is made available under a CC-BY-NC 4.0 International license.

767 when the exon skipping efficiency was above 70% at the top, and Spearman correlation between all skipped
768 and unskipped conditions at the bottom; ****p-value < 0.0001, ns: not significant).

769 **Figure S5 – Comparison of hiPSC-derived and tissue-derived MyoT for the expression of cell cycle genes and**
770 **myogenic regulators.** Hierarchical clustering and heatmap of **A)** selected cell cycle transcripts and miRNAs, and
771 **B)** DLK1, IGF2 and selected myosin transcripts in hiPSCs (D0), hiPSC- and tissue-derived MyoT. **C)** Dotplot of
772 DMD/healthy expression ratio of muscle transcription factors. Significant statistical differences are shown in
773 brackets (*adjusted p-value ≤ 0.05, **adjusted p-value ≤ 0.01, ***adjusted p-value ≤ 0.001, ****adjusted p-
774 value ≤ 0.0001). (hiPSC: human induced pluripotent stem cell; MyoT: myotube).

775 **Figure S6 – Dysregulations of metabolic pathways and mitochondrial genes during differentiation of DMD**
776 **hiPSCs. A)** Scheme of metabolism dysregulations at day 25. Dotplots of **B)** mitochondrial transcripts, **C)**
777 transcripts coding mitochondrial protein import, and **D)** transcripts coding mitochondrial
778 transcription/replication; **E)** Mitochondrial DNA quantification by qPCR at D25. Dotplots of mitochondrial
779 proteins expressed at D17 involved in **F)** protein import, **G)** mitochondrial transcription/replication. Statistics
780 are in brackets (*adjusted p-value ≤ 0.05, **adjusted p-value ≤ 0.01, ***adjusted p-value ≤ 0.001,
781 ****adjusted p-value ≤ 0.0001; D: day).

bioRxiv preprint doi: https://doi.org/10.1101/720920. The copyright holder for this preprint (which was not peer-reviewed) is the author/funder. It is made available under a CC-BY-NC 4.0 International license.

782 **REFERENCES**

783 1. Hoffman EP, Brown RH, Kunkel LM. Dystrophin: the protein product of the Duchenne muscular dystrophy locus. Cell.
784 1987;51(6):919–28.

785 2. Koeks Z, Bladen CL, Salgado D, van Zwet E, Pogoryelova O, McMacken G, et al. Clinical Outcomes in Duchenne Muscular
786 Dystrophy: A Study of 5345 Patients from the TREAT-NMD DMD Global Database. J Neuromuscul Dis [Internet]. 2017;4(4):293–
787 306. Available from:
788 http://www.ncbi.nlm.nih.gov/pubmed/29125504%0Ahttp://www.pubmedcentral.nih.gov/articlerender.fcgi?artid=PMC5701764

789 3. Liu M, Chino N, Ishihara T. Muscle damage progression in Duchenne muscular dystrophy evaluated by a new quantitative
790 computed tomography method. Arch Phys Med Rehab. 1993;74(5):507–14.

791 4. Pescatori M, Broccolini A, Minetti C, Bertini E, Bruno C, D'amico A, et al. Gene expression profiling in the early phases of {DMD:}
792 a constant molecular signature characterizes {DMD} muscle from early postnatal life throughout disease progression. {FASEB} J.
793 2007;21(4):1210–26.

794 5. Szigyarto C, Spitali P. Biomarkers of Duchenne muscular dystrophy: current findings. Degener Neurol Neuromuscul Dis.
795 2018;8:1–13.

796 6. Moat SJ, Bradley DM, Salmon R, Clarke A, Hartley L. Newborn bloodspot screening for Duchenne muscular dystrophy: 21 years
797 experience in Wales {(UK).}. Eur J Hum Genet. 2013;21(10):1049–53.

798 7. Crone M, Mah JK. Current and Emerging Therapies for Duchenne Muscular Dystrophy. Curr Treat Options Neurol. 2018;20(8):31.

799 8. Ngoc L-N, Malerba A, Popplewell L, Schnell F, Hanson G, Dickson G. Systemic Antisense Therapeutics for Dystrophin and
800 Myostatin Exon Splice Modulation Improve Muscle Pathology of Adult mdx Mice. Mol Ther - Nucleic Acids. 2017;6:15–28.

801 9. Nguyen F, Cherel Y, Guigand L, I G-L, Wyers M. Muscle lesions associated with dystrophin deficiency in neonatal golden retriever
802 puppies. J Comp Pathol. 2002;126(2–3):100–8.

803 10. Bassett DI. Dystrophin is required for the formation of stable muscle attachments in the zebrafish embryo. Development.
804 2003;130(23):5851–60.

805 11. Merrick D, Stadler LK, Larner D, Smith J. Muscular dystrophy begins early in embryonic development deriving from stem cell loss
806 and disrupted skeletal muscle formation. Dis Model Mech. 2009;2(7–8):374–88.

807 12. Emery AE. Muscle histology and creatine kinase levels in the foetus in Duchenne muscular dystrophy. Nature.
808 1977;266(5601):472–3.

809 13. Toop J, Emery AE. Muscle histology in fetuses at risk for Duchenne muscular dystrophy. Clin Genet. 1974;5(3):230–3.

810 14. Vassilopoulos D, Emery AE. Muscle nuclear changes in fetuses at risk for Duchenne muscular dystrophy. J Med Genet.
811 1977;14(1):13–5.

812 15. Massouridès E, Polentes J, Mangeot PE, Mournetas V, Nectoux J, Deburgrave N, et al. Dp412e: A novel human embryonic

bioRxiv preprint doi: https://doi.org/10.1101/720920. The copyright holder for this preprint (which was not peer-reviewed) is the author/funder. It is made available under a CC-BY-NC 4.0 International license.

813 dystrophin isoform induced by BMP4 in early differentiated cells. Skelet Muscle [Internet]. 2015 Dec 14 [cited 2017 Feb
814 27];5(1):40. Available from: http://www.skeletalmusclejournal.com/content/5/1/40

815 16. Nesmith AP, Wagner MA, Pasqualini FS, B OB, Pincus MJ, August PR, et al. A human in vitro model of Duchenne muscular
816 dystrophy muscle formation and contractility. J Cell Biol. 2016;215(1):47–56.

817 17. Shoji E, Sakurai H, Nishino T, Nakahata T, Heike T, Awaya T, et al. Early pathogenesis of Duchenne muscular dystrophy modelled
818 in patient-derived human induced pluripotent stem cells. Sci Rep. 2015;5:12831.

819 18. Choi IY, Lim HT, Estrellas K, Mula J, Cohen T V., Zhang Y, et al. Concordant but Varied Phenotypes among Duchenne Muscular
820 Dystrophy Patient-Specific Myoblasts Derived using a Human iPSC-Based Model. Cell Rep. 2016;15(10):2301–12.

821 19. Chal J, Oginuma M, Al Tanoury Z, Gobert B, Sumara O, Hick A, et al. Differentiation of pluripotent stem cells to muscle fiber to
822 model Duchenne muscular dystrophy. Nat Biotechnol. 2015;33(9):962–9.

823 20. Young CS, Hicks MR, Ermolova N V, Nakano H, Jan M, Younesi S, et al. A Single {CRISPR-Cas9} Deletion Strategy that Targets the
824 Majority of {DMD} Patients Restores Dystrophin Function in {hiPSC-Derived} Muscle Cells. Cell Stem Cell. 2016;18(4):533–40.

825 21. Hicks MR, Hiserodt J, Paras K, Fujiwara W, Eskin A, Jan M, et al. {ERBB3} and {NGFR} mark a distinct skeletal muscle progenitor
826 cell in human development and {hPSCs.}. Nat Cell Biol. 2018;20(1):46–57.

827 22. Kodaka Y, Rabu G, Asakura A. Skeletal Muscle Cell Induction from Pluripotent Stem Cells. Stem Cells Int. 2017;2017:1376151.

828 23. Caron L, Kher D, Lee KL, McKernan R, Dumevska B, Hidalgo A, et al. A Human Pluripotent Stem Cell Model of
829 Facioscapulohumeral Muscular Dystrophy-Affected Skeletal Muscles. Stem Cells Transl Med. 2016;5(9):1145–61.

830 24. Shelton M, Metz J, Liu J, Carpenedo RL, Demers S-PP, Stanford WL, et al. Derivation and expansion of {PAX7-positive} muscle
831 progenitors from human and mouse embryonic stem cells. Stem Cell Reports. 2014;3(3):516–29.

832 25. Xi H, Fujiwara W, Gonzalez K, Jan M, Liebscher S, Van Handel B, et al. {In~Vivo} Human Somitogenesis Guides Somite
833 Development from {hPSCs.}. Cell Rep. 2017;18(6):1573–85.

834 26. Monaco AP, Neve RL, Chris C-F, Bertelson CJ, Kurnit DM, Kunkel LM. Isolation of candidate {cDNAs} for portions of the Duchenne
835 muscular dystrophy gene. Nature. 1986;323(6089):646–50.

836 27. Byers TJ, Lidov HGW, Kunkel LM. An alternative dystrophin transcript specific to peripheral nerve. Nat Genet. 1993;4(1):ng0593-
837 77.

838 28. Lidov HG, Selig S, Kunkel LM. Dp140: a novel 140 {kDa} {CNS} transcript from the dystrophin locus. Hum Mol Genet.
839 1995;4(3):329–35.

840 29. Górecki DC, Monaco AP, Derry JM, Walker AP, Barnard EA, Barnard PJ. Expression of four alternative dystrophin transcripts in
841 brain regions regulated by different promoters. Hum Mol Genet. 1992;1(7):505–10.

842 30. D'souza VN, Man NT, Morris GE, Karges W, Pillers DAM, Ray PN. A novel dystrophin isoform is required for normal retinal
843 electrophysiology. Hum Mol Genet. 1995;4(5):837–42.

bioRxiv preprint doi: https://doi.org/10.1101/720920. The copyright holder for this preprint (which was not peer-reviewed) is the author/funder. It is made available under a CC-BY-NC 4.0 International license.

844 31. Heikinheimo M, Scandrett JM, Wilson DB. Localization of Transcription Factor GATA-4 to Regions of the Mouse Embryo Involved
845 in Cardiac Development. Dev Biol. 1994;164(2):361–73.

846 32. Pfeffer PL, Gerster T, Lun K, Brand M, Busslinger M. Characterization of three novel members of the zebrafish Pax2/5/8 family:
847 dependency of Pax5 and Pax8 expression on the Pax2.1 (noi) function. Development [Internet]. 1998;125(16):3063–74. Available
848 from: http://www.ncbi.nlm.nih.gov/pubmed/9671580

849 33. Chapman DL, Cooper-Morgan A, Harrelson Z, Papaioannou VE. Critical role for Tbx6 in mesoderm specification in the mouse
850 embryo. Mech Dev. 2003;120(7):837–47.

851 34. Hart AH, Hartley L, Sourris K, Stadler ES, Li R, Stanley EG, et al. Mixl1 is required for axial mesendoderm morphogenesis and
852 patterning in the murine embryo. Development [Internet]. 2002;129(15):3597–608. Available from:
853 http://www.ncbi.nlm.nih.gov/pubmed/12117810

854 35. Kanai-Azuma M, Kanai Y, Gad JM, Tajima Y, Taya C, Kurohmaru M, et al. Depletion of definitive gut endoderm in Sox17-null
855 mutant mice. Development [Internet]. 2002;129(10):2367–79. Available from: http://www.ncbi.nlm.nih.gov/pubmed/11973269

856 36. Rex M, Orme A, Uwanogho D, Tointon K, Wigmore PM, Sharpe PT, et al. Dynamic expression of chicken Sox2 and Sox3 genes in
857 ectoderm induced to form neural tissue. Dev Dyn. 1997;209(3):323–32.

858 37. Machon O, Masek J, Machonova O, Krauss S, Kozmik Z. Meis2 is essential for cranial and cardiac neural crest development. BMC
859 Dev Biol. 2015;15(1):40.

860 38. Laing NG, Dye DE, Wallgren-Pettersson C, Richard G, Monnier N, Lillis S, et al. Mutations and polymorphisms of the skeletal
861 muscle α-actin gene (ACTA1). Hum Mutat. 2009;30(9):1267–77.

862 39. Kardon G, Heanue TA, Tabin CJ. Pax3 and Dach2 positive regulation in the developing somite. Dev Dyn. 2002;224(3):350–5.

863 40. Pereira FA, Yuhong Q, Zhou G, Tsai MJ, Tsai SY. The orphan nuclear receptor COUP-TFII is required for angiogenesis and heart
864 development. Genes Dev. 1999;13(8):1037–49.

865 41. Mitsiadis TA, Salmivirta M, Muramatsu T, Muramatsu H, Rauvala H, Lehtonen E, et al. Expression of the heparin-binding
866 cytokines, midkine (MK) and HB-GAM (pleiotrophin) is associated with epithelial-mesenchymal interactions during fetal
867 development and organogenesis. Development [Internet]. 1995;121(1):37–51. Available from:
868 http://www.ncbi.nlm.nih.gov/pubmed/7867507

869 42. Yang XM, Vogan K, Gros P, Park M. Expression of the met receptor tyrosine kinase in muscle progenitor cells in somites and limbs
870 is absent in Splotch mice. Development [Internet]. 1996;122(7):2163–71. Available from:
871 http://www.ncbi.nlm.nih.gov/pubmed/8681797

872 43. Sasaki H, Ferguson-Smith AC, Shum AS, Barton SC, Surani MA. Temporal and spatial regulation of H19 imprinting in normal and
873 uniparental mouse embryos. Development [Internet]. 1995;121(12):4195–202. Available from:
874 http://www.ncbi.nlm.nih.gov/pubmed/8575319

875 44. Borycki AG, Mendham L, Emerson CP. Control of somite patterning by Sonic hedgehog and its downstream signal response

bioRxiv preprint doi: https://doi.org/10.1101/720920. The copyright holder for this preprint (which was not peer-reviewed) is the author/funder. It is made available under a CC-BY-NC 4.0 International license.

876 genes. Development [Internet]. 1998;125(4):777–90. Available from: http://www.ncbi.nlm.nih.gov/pubmed/9435297

877 45. Lee CS, Buttitta L, Fan C-M. Evidence that the {WNT-inducible} growth arrest-specific gene 1 encodes an antagonist of sonic
878 hedgehog signaling in the somite. Proc Natl Acad Sci. 2001;98(20):11347–52.

879 46. McMahon AR, Merzdorf CS. Expression of the zic1, zic2, zic3, and zic4 genes in early chick embryos. BMC Res Notes.
880 2010;3(1):167.

881 47. Bladt F, Riethmacher D, Isenmann S, Aguzzi A, Birchmeier C. Essential role for the c-met receptor in the migration of myogenic
882 precursor cells into the limb bud. Nature. 1995;376(6543):768–71.

883 48. Swartz ME, Eberhart J, Pasquale EB, Krull CE. EphA4/ephrin-A5 interactions in muscle precursor cell migration in the avian
884 forelimb. Development [Internet]. 2001;128(23):4669–80. Available from: http://www.ncbi.nlm.nih.gov/pubmed/11731448

885 49. Schäfer K, Braun T. Early specification of limb muscle precursor cells by the homeobox gene Lbx1h. Nat Genet.
886 1999;23(2):ng1099_213.

887 50. Crossley PH, Minowada G, MacArthur CA, Martin GR. Roles for FGF8 in the induction, initiation, and maintenance of chick limb
888 development. Cell. 1996;84(1):127–36.

889 51. Stewart RA, Arduini BL, Berghmans S, George RE, Kanki JP, Henion PD, et al. Zebrafish foxd3 is selectively required for neural
890 crest specification, migration and survival. Dev Biol. 2006;292(1):174–88.

891 52. Deutsch U, Dressler GR, Gruss P. Pax 1, a member of a paired box homologous murine gene family, is expressed in segmented
892 structures during development. Cell. 1988;53(4):617–25.

893 53. Buchner G, Broccoli V, Bulfone A, Orfanelli U, Gattuso C, Ballabio A, et al. {MAEG,} an {EGF-repeat} containing gene, is a new
894 marker associated with dermatome specification and morphogenesis of its derivatives. Mech Dev. 2000;98(1–2):179–82.

895 54. Xu X-M, Fisher DA, Zhou L, White FA, Ng S, Snider WD, et al. The Transmembrane Protein Semaphorin {6A} Repels Embryonic
896 Sympathetic Axons. J Neurosci. 2000;20(7):2638–48.

897 55. Davis RL, Weintraub H, Lassar AB. Expression of a single transfected cDNA converts fibroblasts to myoblasts. Cell.
898 1987;51(6):987–1000.

899 56. Donalies M, Cramer M, Ringwald M, A S-P. Expression of M-cadherin, a member of the cadherin multigene family, correlates
900 with differentiation of skeletal muscle cells. Proc Natl Acad Sci. 1991;88(18):8024–8.

901 57. Gahlmann R, Kedes L. Cloning, structural analysis, and expression of the human fast twitch skeletal muscle troponin C gene. J
902 Biol Chem. 1990;265(21):12520–8.

903 58. Roberds SL, Anderson RD, Ibraghimov-Beskrovnaya O, Campbell KP. Primary structure and muscle-specific expression of the 50-
904 kDa dystrophin-associated glycoprotein (adhalin). J Biol Chem [Internet]. 1993;268(32):23739–42. Available from:
905 http://www.ncbi.nlm.nih.gov/pubmed/8226900

906 59. MacKenzie AE, Korneluk RG, Zorzato F, Fujii J, Phillips M, Iles D, et al. The human ryanodine receptor gene: its mapping to

bioRxiv preprint doi: https://doi.org/10.1101/720920. The copyright holder for this preprint (which was not peer-reviewed) is the author/funder. It is made available under a CC-BY-NC 4.0 International license.

907 19q13.1, placement in a chromosome 19 linkage group, and exclusion as the gene causing myotonic dystrophy. Am J Hum Genet
908 [Internet]. 1990;46(6):1082–9. Available from:
909 http://www.ncbi.nlm.nih.gov/pubmed/1971150%0Ahttp://www.pubmedcentral.nih.gov/articlerender.fcgi?artid=PMC1683814

910 60. Greco S, De Simone M, Colussi C, Zaccagnini G, Fasanaro P, Pescatori M, et al. Common {micro-RNA} signature in skeletal muscle
911 damage and regeneration induced by Duchenne muscular dystrophy and acute ischemia. {FASEB} J. 2009;23(10):3335–46.

912 61. Milet C, Duprez D. The Mkx homeoprotein promotes tenogenesis in stem cells and improves tendon repair. Ann Transl Med.
913 2015;3(Suppl 1):S33.

914 62. Lefebvre V, Li P, De Crombrugghe B. A new long form of Sox5 (L-Sox5), Sox6 and Sox9 are coexpressed in chondrogenesis and
915 cooperatively activate the type II collagen gene. EMBO J. 1998;17(19):5718–33.

916 63. NODA M, DENHARDT DT. Regulation of Osteopontin Gene Expression in Osteoblasts. Ann N Y Acad Sci. 1995;760(1):242–8.

917 64. Atala A. Re: Sall1 Maintains Nephron Progenitors and Nascent Nephrons by Acting as Both an Activator and a Repressor: Editorial
918 Comment. J Urol. 2015;194(2):592–3.

919 65. Lytton J, DH M. Molecular cloning of {cDNAs} from human kidney coding for two alternatively spliced products of the cardiac
920 {Ca2+-ATPase} gene. J Biol Chem. 1988;263(29):15024–31.

921 66. Yoshida M, Ozawa E. Glycoprotein complex anchoring dystrophin to sarcolemma. J Biochem. 1990;108(5):748–52.

922 67. Chen JF, Mandel EM, Thomson JM, Wu Q, Callis TE, Hammond SM, et al. The role of microRNA-1 and microRNA-133 in skeletal
923 muscle proliferation and differentiation. Nat Genet. 2006;38(2):228–33.

924 68. Hak KK, Yong SL, Sivaprasad U, Malhotra A, Dutta A. Muscle-specific microRNA miR-206 promotes muscle differentiation. J Cell
925 Biol. 2006;174(5):677–87.

926 69. Hasty P, Bradley A, Morris JH, Edmondson DG, Venuti JM, Olson EN, et al. Muscle deficiency and neonatal death in mice with a
927 targeted mutation in the myogenin gene. Nature. 1993;364(6437):364501a0.

928 70. Vignier N, Moghadaszadeh B, Gary F, Beckmann J, Mayer U, Guicheney P. Structure, genetic localization, and identification of the
929 cardiac and skeletal muscle transcripts of the human integrin α7 gene (ITGA7). Biochem Biophys Res Commun. 1999;260(2):357–
930 64.

931 71. Newey SE, Howman E V., Ponting CP, Benson MA, Nawrotzki R, Loh NY, et al. Syncoilin, a Novel Member of the Intermediate
932 Filament Superfamily That Interacts with α-Dystrobrevin in Skeletal Muscle. J Biol Chem. 2001;276(9):6645–55.

933 72. WU Q-L, JHA PK, RAYCHOWDHURY MK, DU Y, LEAVIS PC, SARKAR S. Isolation and Characterization of Human Fast Skeletal β
934 Troponin T cDNA: Comparative Sequence Analysis of Isoforms and Insight into the Evolution of Members of a Multigene Family.
935 DNA Cell Biol. 2009;13(3):217–33.

936 73. Bernick EP, Zhang PJ, Du S. Knockdown and overexpression of Unc-45b result in defective myofibril organization in skeletal
937 muscles of zebrafish embryos. BMC Cell Biol. 2010;11(1):70.

bioRxiv preprint doi: https://doi.org/10.1101/720920. The copyright holder for this preprint (which was not peer-reviewed) is the author/funder. It is made available under a CC-BY-NC 4.0 International license.

938 74. Li H, Randall WR, Du S-J. skNAC (skeletal Naca), a muscle-specific isoform of Naca (nascent polypeptide-associated complex
939 alpha), is required for myofibril organization. FASEB J. 2009;23(6):1988–2000.

940 75. DeChiara TM, Bowen DC, Valenzuela DM, Simmons M V., Poueymirou WT, Thomas S, et al. The receptor tyrosine kinase MuSK is
941 required for neuromuscular junction formation in vivo. Cell. 1996;85(4):501–12.

942 76. Okada K, Inoue A, Okada M, Murata Y, Kakuta S, Jigami T, et al. The Muscle Protein Dok-7 Is Essential for Neuromuscular
943 Synaptogenesis. Science (80-). 2006;312(5781):1802–5.

944 77. Ilene K-M, Travis M, Blau H, Leinwand LA. Expression and {DNA} sequence analysis of a human embryonic skeletal muscle mvosin
945 heavy chain gene. Nucleic Acids Res. 1989;17(15):6167–79.

946 78. Weiss A, Schiaffino S, Leinwand LA. Comparative sequence analysis of the complete human sarcomeric myosin heavy chain
947 family: implications for functional {diversity11Edited} by J. Karn. J Mol Biol. 1999;290(1):61–75.

948 79. Strohman RC, J M-E, Glass CA, Matsuda R. Human fetal muscle and cultured myotubes derived from it contain a fetal-specific
949 myosin light chain. Science (80-). 1983;221(4614):955–7.

950 80. Collins C, Hayden MR, Schappert K. The genomic organization of a novel regulatory myosin light chain gene (MYL5) that maps to
951 chromosome 4p16.3 and shows different patterns of expression between primates. Hum Mol Genet. 1992;1(9):727–33.

952 81. Type IIx myosin heavy chain transcripts are expressed in type IIb fibers of human skeletal muscle. Am J Physiol - Cell Physiol.
953 1994;267(6 36-6):C1723-8.

954 82. Rotwein P, Pollock KM, Watson M, Milbrandt JD. Insulin-like growth factor gene expression during rat embryonic development.
955 Endocrinology. 1987;121(6):2141–4.

956 83. Andersen DC, Laborda J, Baladron V, Kassem M, Sheikh SP, Jensen CH. Dual role of delta-like 1 homolog (DLK1) in skeletal muscle
957 development and adult muscle regeneration. Development. 2013;140(18):3743–53.

958 84. Noguchi S, EM M, Othmane BK, Hagiwara Y, Mizuno Y, Yoshida M, et al. Mutations in the dystrophin-associated protein gamma-
959 sarcoglycan in chromosome 13 muscular dystrophy. Sci New York N Y. 1995;270(5237):819–22.

960 85. Campbell KP, Leung AT, Sharp AH. The biochemistry and molecular biology of the dihydropyridine-sensitive calcium channel.
961 Trends Neurosci. 1988;11(10):425–30.

962 86. A fourth human MEF2 transcription factor, hMEF2D, is an early marker of the myogenic lineage. Development.
963 1993;118(4):1095–106.

964 87. Gautam M, Noakes PG, Mudd J, Nichol M, Chu GC, Sanes JR, et al. Failure of postsynaptic specialization to develop at
965 neuromuscular junctions of rapsyn-deficient mice. Nature. 1995;377(6546):377232a0.

966 88. Dawson DM, Eppenberger HM, Eppenberger ME. Multiple Molecular Forms of Creatine Kinases. Ann N Y Acad Sci.
967 1968;151(1):616–26.

968 89. van Rooij E, Sutherland LB, Qi X, Richardson JA, Hill J, Olson EN. Control of {Stress-Dependent} Cardiac Growth and Gene

bioRxiv preprint doi: https://doi.org/10.1101/720920. The copyright holder for this preprint (which was not peer-reviewed) is the author/funder. It is made available under a CC-BY-NC 4.0 International license.

969 Expression by a {MicroRNA}. Science (80-). 2007;316(5824):575–9.

970 90. Hailstones D, Barton P, P C-T, Sasse S, Sutherland C, Hardeman E, et al. Differential regulation of the atrial isoforms of the myosin
971 light chains during striated muscle development. J Biol Chem. 1992;267(32):23295–300.

972 91. Marx SO, Reiken S, Hisamatsu Y, Jayaraman T, Burkhoff D, Rosemblit N, et al. PKA Phosphorylation Dissociates FKBP12.6 from
973 the Calcium Release Channel (Ryanodine Receptor). Cell. 2004;101(4):365–76.

974 92. Kuro-o M, Nagai R, Tsuchimochi H, Katoh H, Yazaki Y, Ohkubo A, et al. Developmentally regulated expression of vascular smooth
975 muscle myosin heavy chain isoforms. J Biol Chem. 1989;264(31):18272–5.

976 93. Gimona M, Herzog M, Vandekerckhove J, Small JV. Smooth muscle specific expression of calponin. FEBS Lett. 1990;274(1–
977 2):159–62.

978 94. Eglen RM, Reddy H, Watson N, Challiss RAJ. Muscarinic acetylcholine receptor subtypes in smooth muscle. Trends Pharmacol Sci.
979 1994;15(4):114–9.

980 95. Ajima R, Akazawa H, Kodama M, Takeshita F, Otsuka A, Kohno T, et al. Deficiency of Myo18B in mice results in embryonic
981 lethality with cardiac myofibrillar aberrations. Genes to Cells. 2008;13(10):987–99.

982 96. Heidmann O, Buonanno A, Geoffroy B, Robert B, Guenet JL, Merlie JP, et al. Chromosomal localization of muscle nicotinic
983 acetylcholine receptor genes in the mouse. Science (80-). 1986;234(4778):866–8.

984 97. Capitanio D, Moriggi M, Torretta E, Barbacini P, Palma S, Viganò A, et al. Comparative proteomic analyses of Duchenne muscular
985 dystrophy and Becker muscular dystrophy muscles: changes contributing to preserve muscle function in Becker muscular
986 dystrophy patients. 2020;

987 98. Ueno T, Tanaka K, Kaneko K, Taga Y, Sata T, Irie S, et al. Enhancement of procollagen biosynthesis by p180 through augmented
988 ribosome association on the endoplasmic reticulum in response to stimulated secretion. J Biol Chem. 2010;285(39):29941–50.

989 99. Hautala T, Byers MG, Eddy RL, Shows TB, Kivirikko KI, Myllyla R. Cloning of human lysyl hydroxylase: Complete cDNA-derived
990 amino acid sequence and assignment of the gene (PLOD) to chromosome 1p36.3→p36.2. Genomics. 1992;13(1):62–9.

991 100. Valtavaara M, Papponen H, Pirttilä AM, Hiltunen K, Helander H, Myllylä R. Cloning and characterization of a novel human lysyl
992 hydroxylase isoform highly expressed in pancreas and muscle. J Biol Chem. 1997;272(11):6831–4.

993 101. Martens JHA, Verlaan M, Kalkhoven E, Zantema A. Cascade of Distinct Histone Modifications during Collagenase Gene Activation.
994 Mol Cell Biol. 2003;23(5):1808–16.

995 102. Long DA, Price KL, Ioffe E, Gannon CM, Gnudi L, White KE, et al. Angiopoietin-1 therapy enhances fibrosis and inflammation
996 following folic acid-induced acute renal injury. Kidney Int. 2008;74(3):300–9.

997 103. Lipson KE, Wong C, Teng Y, Spong S. CTGF is a central mediator of tissue remodeling and fibrosis and its inhibition can reverse
998 the process of fibrosis. Fibrogenesis Tissue Repair [Internet]. 2012;5(S1):S24. Available from:
999 https://fibrogenesis.biomedcentral.com/articles/10.1186/1755-1536-5-S1-S24

bioRxiv preprint doi: https://doi.org/10.1101/720920. The copyright holder for this preprint (which was not peer-reviewed) is the author/funder. It is made available under a CC-BY-NC 4.0 International license.

1000 104. Fragiadaki M, Witherden AS, Kaneko T, Sonnylal S, Pusey CD, George B-G, et al. Interstitial fibrosis is associated with increased
1001 {COL1A2} transcription in {AA-injured} renal tubular epithelial cells in vivo. Matrix Biol. 2011;30(7–8):396–403.

1002 105. Hemmann S, Graf J, Roderfeld M, Roeb E. Expression of {MMPs} and {TIMPs} in liver fibrosis – a systematic review with special
1003 emphasis on anti-fibrotic strategies. J Hepatol. 2007;46(5):955–75.

1004 106. Duisters RF, Tijsen AJ, Schroen B, Leenders JJ, Lentink V, Van Der Made I, et al. MiR-133 and miR-30 Regulate connective tissue
1005 growth factor: Implications for a role of micrornas in myocardial matrix remodeling. Circ Res. 2009;104(2):170–8.

1006 107. Vidal B, Serrano AL, Tjwa M, Suelves M, Ardite E, Mori R, et al. Fibrinogen drives dystrophic muscle fibrosis via a
1007 {TGFβ/alternative} macrophage activation pathway. Gene Dev. 2008;22(13):1747–52.

1008 108. Timpani CA, Hayes A, Rybalka E. Revisiting the dystrophin-ATP connection: How half a century of research still implicates
1009 mitochondrial dysfunction in Duchenne Muscular Dystrophy aetiology. Med Hypotheses. 2015;85(6):1021–33.

1010 109. Šileikyte J, Blachly-Dyson E, Sewell R, Carpi A, Menabò R, Di Lisa F, et al. Regulation of the mitochondrial permeability transition
1011 pore by the outer membrane does not involve the peripheral benzodiazepine receptor (translocator protein of 18 kDa (TSPO)). J
1012 Biol Chem. 2014;289(20):13769–81.

1013 110. Emery AE, Burt D. Intracellular calcium and pathogenesis and antenatal diagnosis of Duchenne muscular dystrophy. Br Med J.
1014 1980;280(6211):355–7.

1015 111. Shkryl VM, Martins AS, Ullrich ND, Nowycky MC, Niggli E, Shirokova N. Reciprocal amplification of ROS and Ca2+ signals in
1016 stressed mdx dystrophic skeletal muscle fibers. Pflugers Arch Eur J Physiol. 2009;458(5):915–28.

1017 112. Whitehead NP, Yeung EW, Froehner SC, Allen DG. Skeletal muscle NADPH oxidase is increased and triggers stretch-induced
1018 damage in the mdx mouse. PLoS One. 2010;5(12):e15354.

1019 113. Rodriguez MC, Tarnopolsky MA. Patients with dystrophinopathy show evidence of increased oxidative stress. Free Radic Biol
1020 Med. 2003;34(9):1217–20.

1021 114. Scholte HR, Busch HFM. Early changes of muscle mitochondria in duchenne dystrophy Partition and activity of mitochondrial
1022 enzymes in fractionated muscle of unaffected boys and adults and patients. J Neurol Sci. 1980;45(2–3):217–34.

1023 115. Sharma U, Atri S, Sharma MC, Sarkar C, Jagannathan NR. Skeletal muscle metabolism in Duchenne muscular dystrophy {(DMD):}
1024 an in-vitro proton {NMR} spectroscopy study. Magn Reson Imaging. 2003;21(2):145–53.

1025 116. Lemos DR, Babaeijandaghi F, Low M, Chang C-K, Lee ST, Fiore D, et al. Nilotinib reduces muscle fibrosis in chronic muscle injury
1026 by promoting {TNF-mediated} apoptosis of fibro/adipogenic progenitors. Nat Med. 2015;21(7):786–94.

1027 117. Villalta AS, Nguyen HX, Deng B, Gotoh T, Tidball JG. Shifts in macrophage phenotypes and macrophage competition for arginine
1028 metabolism affect the severity of muscle pathology in muscular dystrophy. Hum Mol Genet. 2009;18(3):482–96.

1029 118. Desguerre I, Mayer M, Leturcq F, Barbet J-P, Gherardi RK, Christov C. Endomysial Fibrosis in Duchenne Muscular Dystrophy: A
1030 Marker of Poor Outcome Associated With Macrophage Alternative Activation. J Neuropathol Exp Neurol. 2009;68(7):762–73.

bioRxiv preprint doi: https://doi.org/10.1101/720920. The copyright holder for this preprint (which was not peer-reviewed) is the author/funder. It is made available under a CC-BY-NC 4.0 International license.

1031 119. Fusako S-T, Narita A, Masuda S, Wakamatsu T, Watanabe N, Nishiyama T, et al. Premyogenic progenitors derived from human
1032 pluripotent stem cells expand in floating culture and differentiate into transplantable myogenic progenitors. Sci Rep-uk.
1033 2018;8(1):6555.

1034 120. Matsumura K, Tome FMS, Ionasescu V, Ervasti JM, Anderson RD, Romero NB, et al. Deficiency of dystrophin-associated proteins
1035 in Duchenne muscular dystrophy patients lacking COOH-terminal domains of dystrophin. J Clin Invest. 1993;92(2):866–71.

1036 121. Yuasa K, Hagiwara Y, Ando M, Nakamura A, Takeda S, Hijikata T. {MicroRNA-206} is highly expressed in newly formed muscle
1037 fibers: implications regarding potential for muscle regeneration and maturation in muscular dystrophy. Cell Struct Funct.
1038 2008;33(2):163–9.

1039 122. Cullen MJ, Fulthorpe JJ. Stages in fibre breakdown in duchenne muscular dystrophy An electron-microscopic study. J Neurol Sci.
1040 1975;24(2):179–200.

1041 123. Brouilly N, Lecroisey C, Martin E, Pierson L, Mariol MC, Mounier N, et al. Ultra-structural time-course study in the C. elegans
1042 model for Duchenne muscular dystrophy highlights a crucial role for sarcomere-anchoring structures and sarcolemma integrity
1043 in the earliest steps of the muscle degeneration process. Hum Mol Genet. 2015;24(22):6428–45.

1044 124. Consolino CM, Brooks S V. Susceptibility to sarcomere injury induced by single stretches of maximally activated muscles of mdx
1045 mice. J Appl Physiol Bethesda Md 1985. 2004;96(2):633–8.

1046 125. Kong J, Anderson JE. Dystrophin is required for organizing large acetylcholine receptor aggregates. Brain Res. 1999;839(2):298–
1047 304.

1048 126. Kong J, Yang L, Li Q, Cao J, Yang J, Chen F, et al. The absence of dystrophin rather than muscle degeneration causes acetylcholine
1049 receptor cluster defects in dystrophic muscle. Neuroreport. 2012;23(2):82–7.

1050 127. Bell CD, Conen PE. Histopathological changes in Duchenne muscular dystrophy. J Neurol Sci. 1968;7(3):529–44.

1051 128. Haddix SG, il Lee Y, Kornegay JN, Thompson WJ. Cycles of myofiber degeneration and regeneration lead to remodeling of the
1052 neuromuscular junction in two mammalian models of Duchenne muscular dystrophy. PLoS One. 2018;13(10):e0205926.

1053 129. Luz MAM, Marques MJ, Neto SH. Impaired regeneration of dystrophin-deficient muscle fibers is caused by exhaustion of
1054 myogenic cells. Braz J Med Biol Res. 2002;35(6):691–5.

1055 130. Zhou L, Porter JD, Cheng G, Gong B, Hatala DA, Merriam AP, et al. Temporal and spatial {mRNA} expression patterns of {TGF-
1056 beta1,} 2, 3 and {TbetaRI,} {II,} {III} in skeletal muscles of mdx mice. Neuromuscul Disord Nmd. 2005;16(1):32–8.

1057 131. Bernasconi P, Torchiana E, Confalonieri P, Brugnoni R, Barresi R, Mora M, et al. Expression of transforming growth factor-beta 1
1058 in dystrophic patient muscles correlates with fibrosis. Pathogenetic role of a fibrogenic cytokine. J Clin Invest. 1995;96(2):1137–
1059 44.

1060 132. Takahashi K, Tanabe K, Ohnuki M, Narita M, Ichisaka T, Tomoda K, et al. Induction of Pluripotent Stem Cells from Adult Human
1061 Fibroblasts by Defined Factors. Cell. 2007;131(5):861–72.

bioRxiv preprint doi: https://doi.org/10.1101/720920. The copyright holder for this preprint (which was not peer-reviewed) is the author/funder. It is made available under a CC-BY-NC 4.0 International license.

1062 133. DREYFUS JC, SCHAPIRA G, SCHAPIRA F. Biochemical study of muscle in progressive muscular dystrophy. J Clin Invest.
1063 1954;33(5):794–7.

1064 134. Ascah A, Khairallah M, Daussin F, Bourcier-Lucas C, Godin R, Allen BG, et al. Stress-induced opening of the permeability transition
1065 pore in the dystrophin-deficient heart is attenuated by acute treatment with sildenafil. Am J Physiol Circ Physiol.
1066 2011;300(1):H144–53.

1067 135. Pauly M, Daussin F, Burelle Y, Li T, Godin R, Fauconnier J, et al. AMPK activation stimulates autophagy and ameliorates muscular
1068 dystrophy in the mdx mouse diaphragm. Am J Pathol. 2012;181(2):583–92.

1069 136. M PC. {HISTOPATHOLOGICAL} {FEATURES} {OF} {MUSCLE} {IN} {THE} {PRECLINICAL} {STAGES} {OF} {MUSCULAR} {DYSTROPHY}.
1070 Brain. 1962;85(1):109–20.

1071 137. Bradley WG, Hudgson P, Larson PF, Papapetropoulos TA, Jenkison M. Structural changes in the early stages of Duchenne
1072 muscular dystrophy. J Neurol Neurosurg Psychiatry. 1972;35(4):451.

1073 138. Rau F, Freyermuth F, Fugier C, Villemin JP, Fischer MC, Jost B, et al. Misregulation of miR-1 processing is associated with heart
1074 defects in myotonic dystrophy. Nat Struct Mol Biol. 2011;18(7):840–5.

1075 139. Singh A, Happel C, Manna SK, George A-M, Carrerero J, Kumar S, et al. Transcription factor {NRF2} regulates {miR-1} and {miR-
1076 206} to drive tumorigenesis. J Clin Invest. 2013;123(7):2921–34.

1077 140. Zhang X, Zuo X, Yang B, Li Z, Xue Y, Zhou Y, et al. MicroRNA directly enhances mitochondrial translation during muscle
1078 differentiation. Cell. 2014;158(3):607–19.

1079 141. Fry CS, Kirby TJ, Kosmac K, McCarthy JJ, Peterson CA. Myogenic Progenitor Cells Control Extracellular Matrix Production by
1080 Fibroblasts during Skeletal Muscle Hypertrophy. Cell Stem Cell. 2017;20(1):56–69.

1081 142. Blau HM, Webster C, Pavlath GK. Defective myoblasts identified in Duchenne muscular dystrophy. Proc Natl Acad Sci.
1082 1983;80(15):4856–60.

1083 143. Bovolenta M, Erriquez D, Valli E, Brioschi S, Scotton C, Neri M, et al. The DMD Locus Harbours Multiple Long Non-Coding RNAs
1084 Which Orchestrate and Control Transcription of Muscle Dystrophin mRNA Isoforms. PLoS One. 2012;7(9).

1085 144. Ervasti JM, Campbell KP. A role for the dystrophin-glycoprotein complex as a transmembrane linker between laminin and actin. J
1086 Cell Biol. 1993;122(4):809–23.

1087 145. Nudel U, Zuk D, Einat P, Zeelon E, Levy Z, Neuman S, et al. Duchenne muscular dystrophy gene product is not identical in muscle
1088 and brain. Nature. 1989;337(6202):337076a0.

1089 146. Muntoni F, Melis MA, Ganau A, Dubowitz V. Transcription of the dystrophin gene in normal tissues and in skeletal muscle of a
1090 family with X-linked dilated cardiomyopathy. Am J Hum Genet. 1995;56(1):151–7.

1091 147. Warner LE. Expression of Dp260 in muscle tethers the actin cytoskeleton to the dystrophin-glycoprotein complex and partially
1092 prevents dystrophy. Hum Mol Genet. 2002;11(9):1095–105.

bioRxiv preprint doi: https://doi.org/10.1101/720920. The copyright holder for this preprint (which was not peer-reviewed) is the author/funder. It is made available under a CC-BY-NC 4.0 International license.

1093 148. Doorenweerd N, Mahfouz A, Van Putten M, Kaliyaperumal R, T'Hoen PAC, Hendriksen JGM, et al. Timing and localization of
1094 human dystrophin isoform expression provide insights into the cognitive phenotype of Duchenne muscular dystrophy. Sci Rep.
1095 2017;7(1).

1096 149. Lu-Nguyen N, Ferry A, Schnell FJ, Hanson GJ, Popplewell L, Dickson G, et al. Functional muscle recovery following dystrophin and
1097 myostatin exon splice modulation in aged mdx mice. Hum Mol Genet. 2019;

1098 150. Peccate C, Mollard A, Le Hir M, Julien L, McClorey G, Jarmin S, et al. Antisense pre-treatment increases gene therapy efficacy in
1099 dystrophic muscles. Hum Mol Genet. 2016;25(16):3555–63.

1100 151. Morales MG, Gutierrez J, Cabello-Verrugio C, Cabrera D, Lipson KE, Goldschmeding R, et al. Reducing CTGF/CCN2 slows down
1101 mdx muscle dystrophy and improves cell therapy. Hum Mol Genet. 2013;22(24):4938–51.

1102 152. Gatliff J, Campanella M. {TSPO:} kaleidoscopic {18-kDa} amid biochemical pharmacology, control and targeting of mitochondria.
1103 Biochem J. 2016;473(2):107–21.

1104 153. Köster J, Rahmann S. Snakemake—a scalable bioinformatics workflow engine. Bioinformatics. 2012;28(19):2520–2.

1105 154. Dobin A, Davis C a, Schlesinger F, Drenkow J, Zaleski C, Jha S, et al. STAR: ultrafast universal RNA-seq aligner. Bioinformatics
1106 [Internet]. 2013 Jan 1 [cited 2014 Jul 13];29(1):15–21. Available from:
1107 http://www.pubmedcentral.nih.gov/articlerender.fcgi?artid=3530905&tool=pmcentrez&rendertype=abstract

1108 155. Wang L, Wang S, Li W. RSeQC: quality control of RNA-seq experiments. Bioinformatics [Internet]. 2012 Aug 15 [cited 2017 Jul
1109 6];28(16):2184–5. Available from: https://academic.oup.com/bioinformatics/article-lookup/doi/10.1093/bioinformatics/bts356

1110 156. Ewels P, Magnusson M, Lundin S, Käller M. MultiQC: Summarize analysis results for multiple tools and samples in a single report.
1111 Bioinformatics [Internet]. 2016 Oct 1 [cited 2017 Jul 6];32(19):3047–8. Available from:
1112 https://academic.oup.com/bioinformatics/article-lookup/doi/10.1093/bioinformatics/btw354

1113 157. Love MI, Huber W, Anders S. Moderated estimation of fold change and dispersion for RNA-seq data with DESeq2. Genome Biol
1114 [Internet]. 2014;15(12):550. Available from: http://genomebiology.biomedcentral.com/articles/10.1186/s13059-014-0550-8

1115 158. Durinck S, Spellman PT, Birney E, Huber W. Mapping identifiers for the integration of genomic datasets with the R/ Bioconductor
1116 package biomaRt. Nat Protoc [Internet]. 2009 [cited 2019 Jun 12];4(8):1184–91. Available from:
1117 http://www.ncbi.nlm.nih.gov/pubmed/19617889

1118 159. Kolesnikov N, Hastings E, Keays M, Melnichuk O, Tang AY, Williams E, et al. {ArrayExpress} update—simplifying data submissions.
1119 Nucleic Acids Res. 2015;43(D1):D1113–6.

1120 160. Schmieder R, Edwards R. Quality control and preprocessing of metagenomic datasets. Bioinformatics. 2011;27(6):863–4.

1121 161. Martin M. Cutadapt removes adapter sequences from high-throughput sequencing reads. Embnet J. 2011;17(1):10–2.

1122 162. Amrhein V, Greenland S, Blake M. Scientists rise up against statistical significance. Nature. 2019;567(7748):305–7.

1123 163. Garnier S. viridis: Default Color Maps from "matplotlib". R package version 0.5.1. 2018; Available from: https://cran.r-

bioRxiv preprint doi: https://doi.org/10.1101/720920. The copyright holder for this preprint (which was not peer-reviewed) is the author/funder. It is made available under a CC-BY-NC 4.0 International license.

1124 project.org/package=viridis

1125 164. Simko TW and V. R package "corrplot": Visualization of a Correlation Matrix (Version 0.84). 2017; Available from:
1126 https://github.com/taiyun/corrplot

1127 165. Gregory R. Warnes, Ben Bolker, Lodewijk Bonebakker, Robert Gentleman, Wolfgang Huber Andy Liaw, Thomas Lumley M,
1128 Maechler, Arni Magnusson, Steffen Moeller MS and BV. gplots: Various R Programming Tools for Plotting Data. R package
1129 version 3.0.1. 2016; Available from: https://cran.r-project.org/package=gplots

1130 166. Fresno C, Fernández EA. {RDAVIDWebService:} a versatile R interface to {DAVID}. Bioinformatics. 2013;29(21):2810–1.

1131 167. Vizcaíno J, Csordas A, del-Toro, Noemi, Dianes JA, Griss J, Lavidas I, et al. 2016 update of the {PRIDE} database and its related
1132 tools. Nucleic Acids Res. 2016;44(D1):D447–56.

1133

Figure 1

bioRxiv preprint doi: https://doi.org/10.1101/720920. The copyright holder for this preprint (which was not peer-reviewed) is the author/funder. It is made available under a CC-BY-NC 4.0 International license.

A

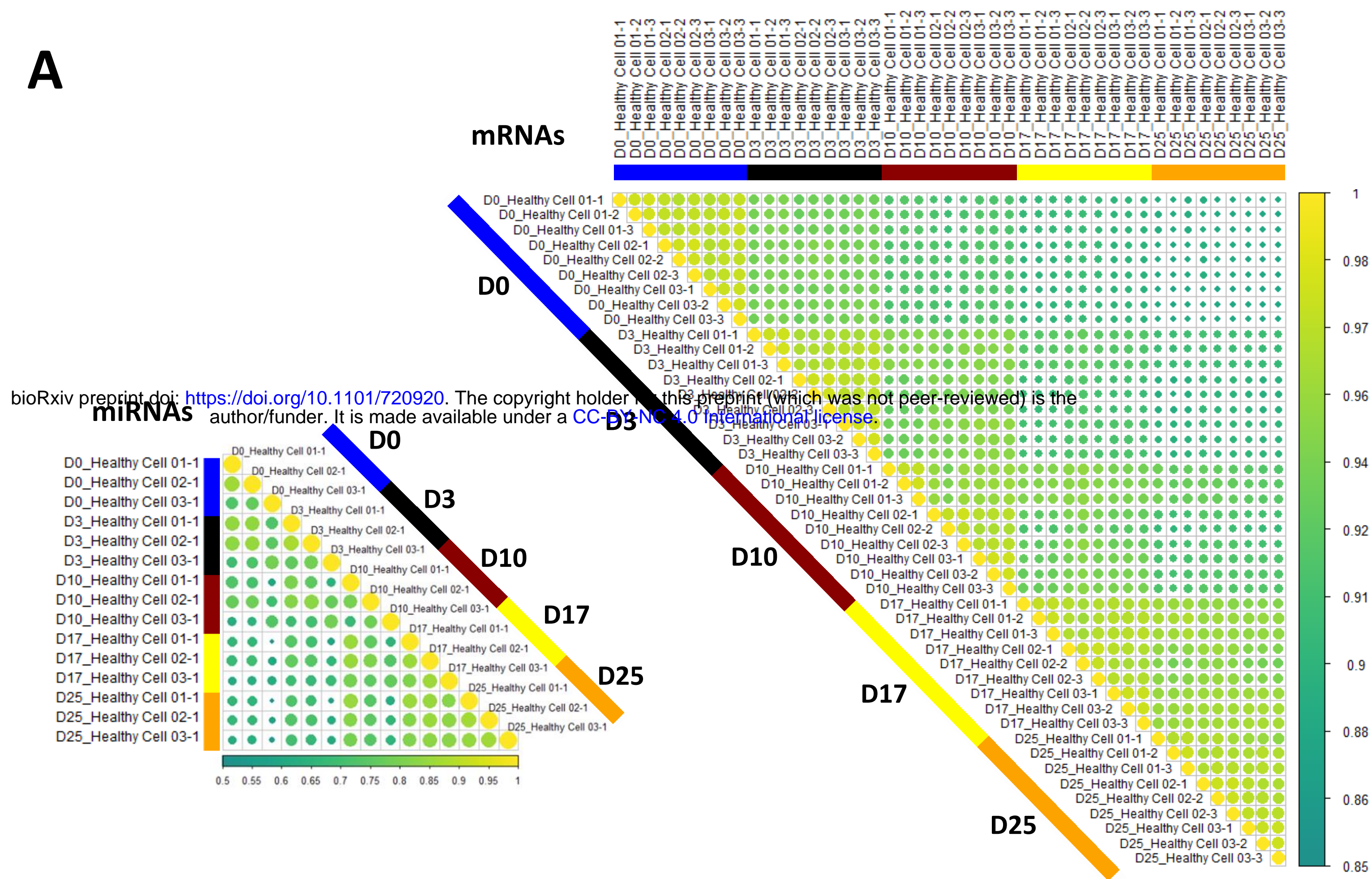

B

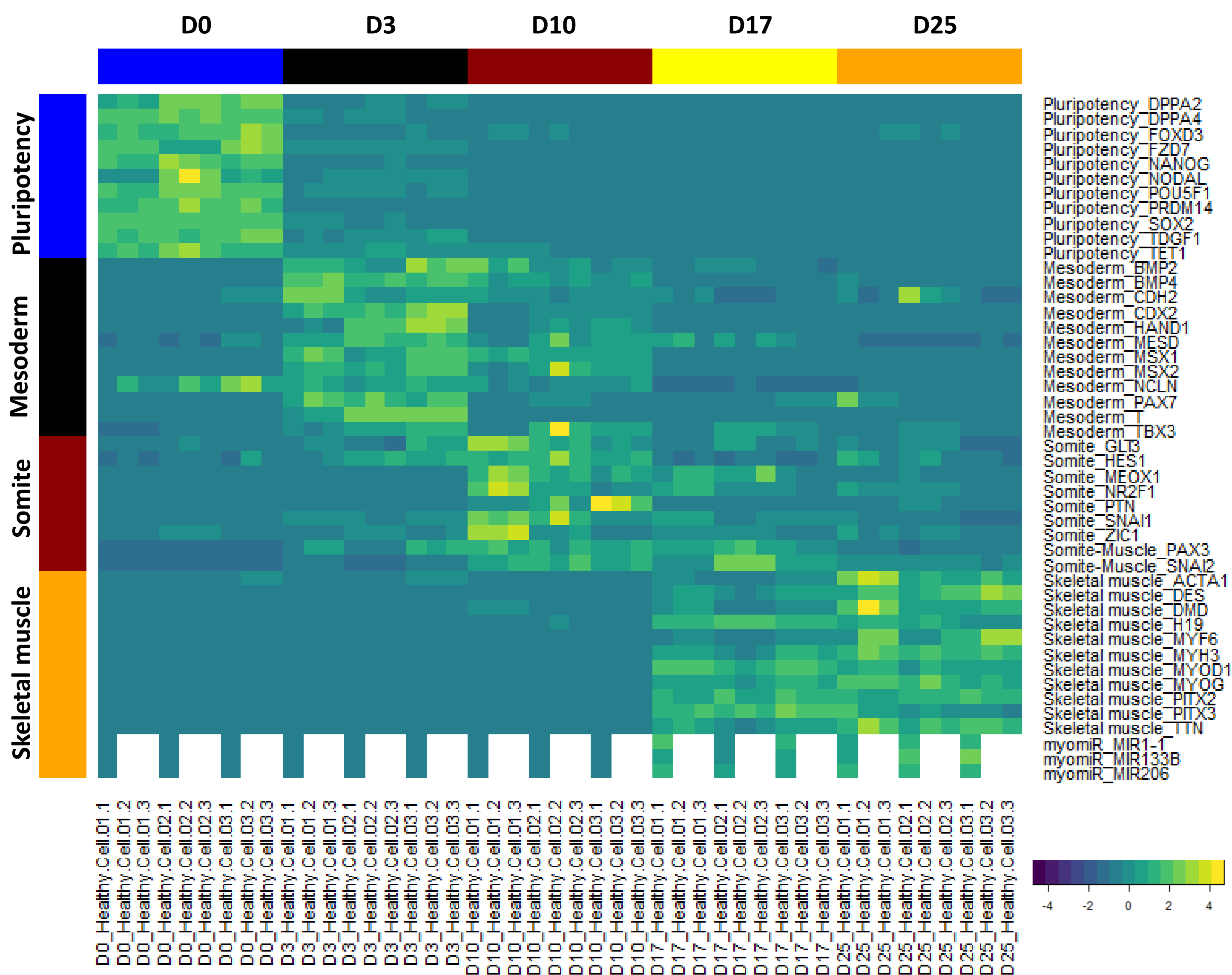

Figure 2

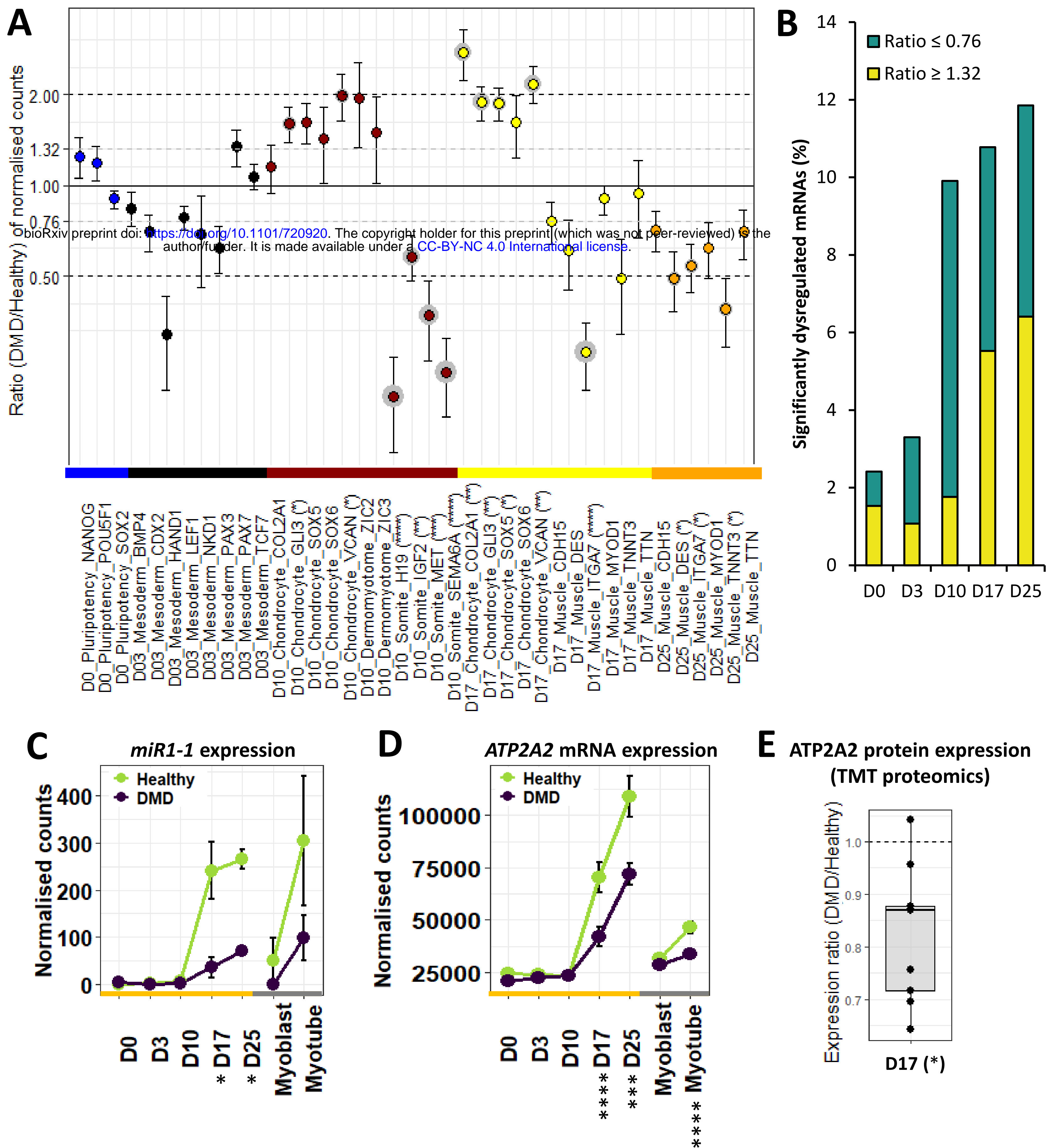

bioRxiv preprint doi: https://doi.org/10.1101/720920. The copyright holder for this preprint (which was not peer-reviewed) is the author/funder. It is made available under a CC-BY-NC 4.0 International license.

Figure 3

bioRxiv preprint doi: https://doi.org/10.1101/720920. The copyright holder for this preprint (which was not peer-reviewed) is the author/funder. It is made available under a CC-BY-NC 4.0 International license.

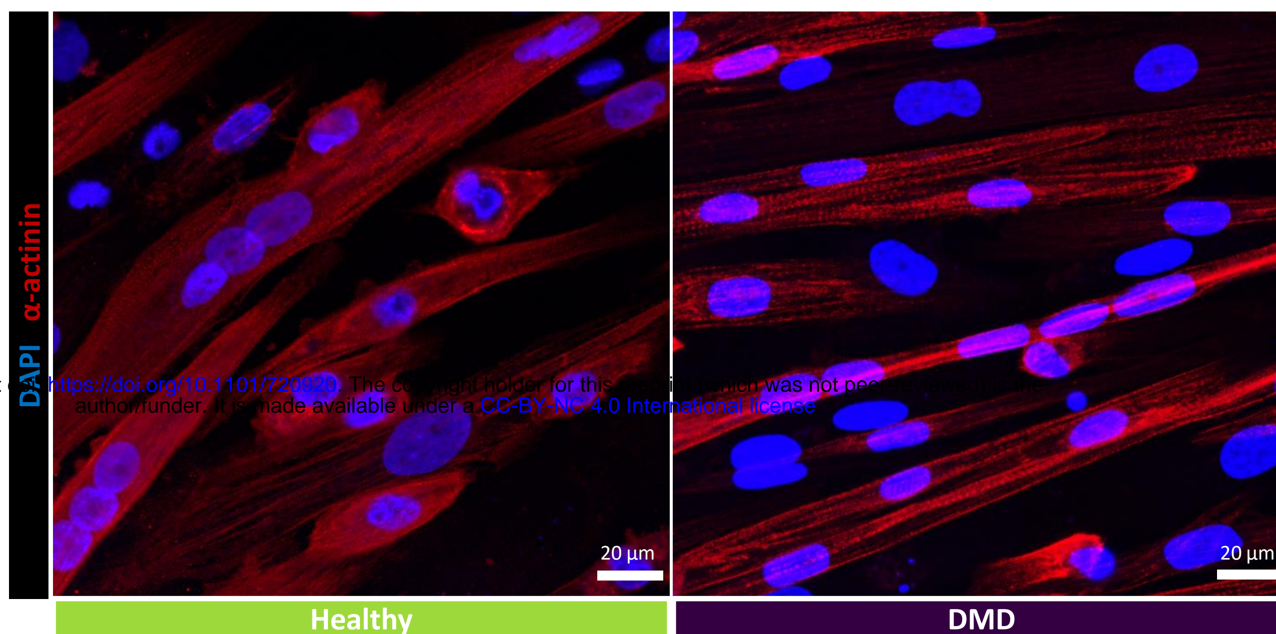

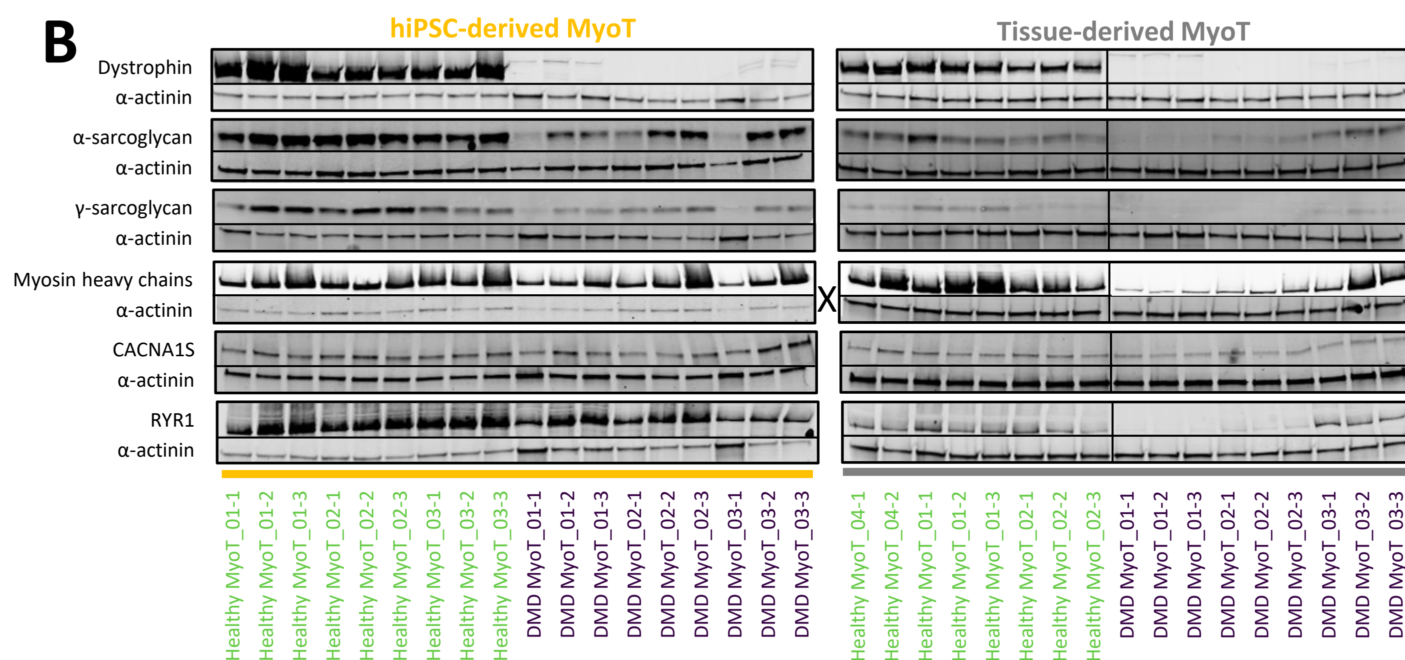

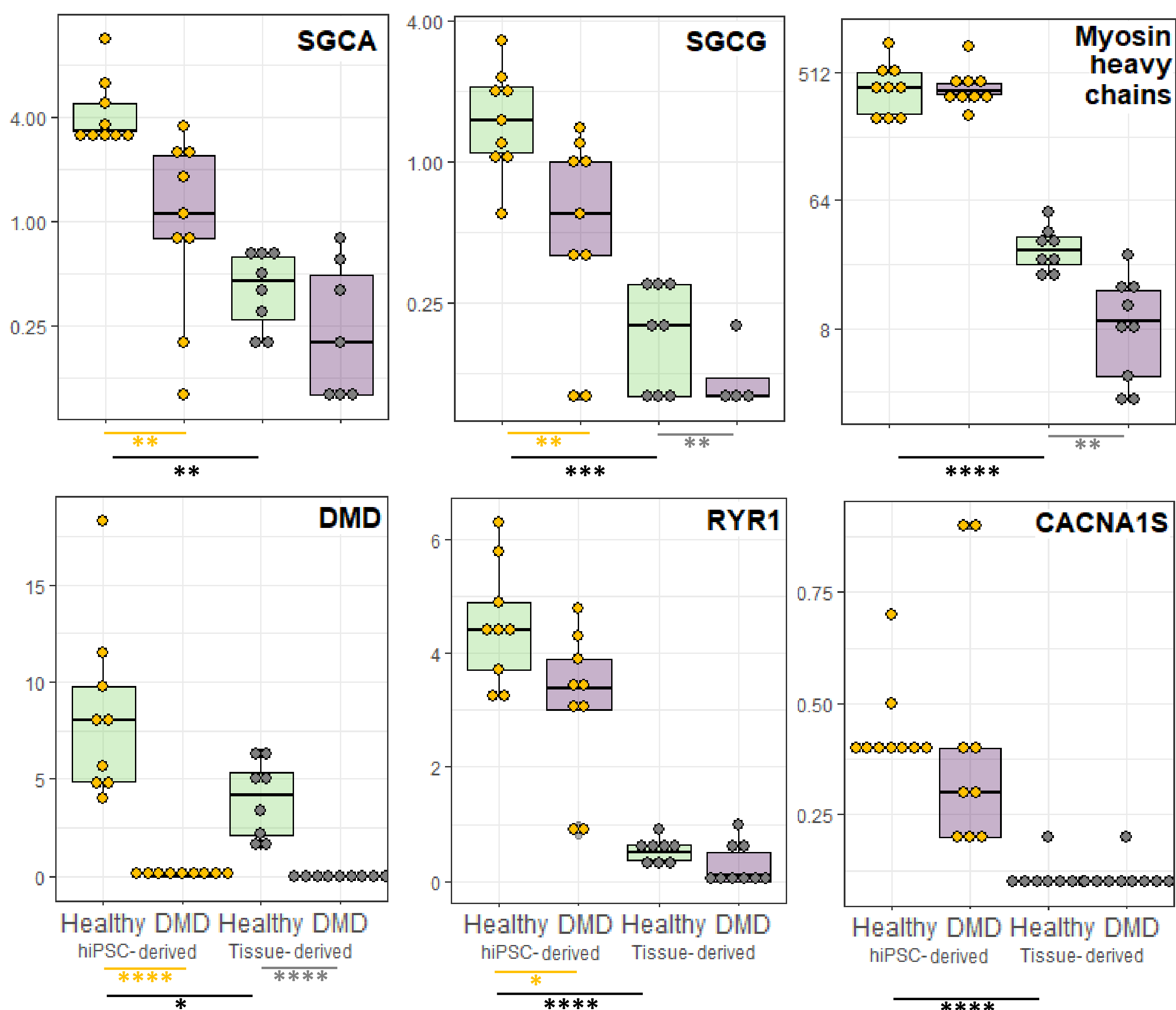

Figure 4

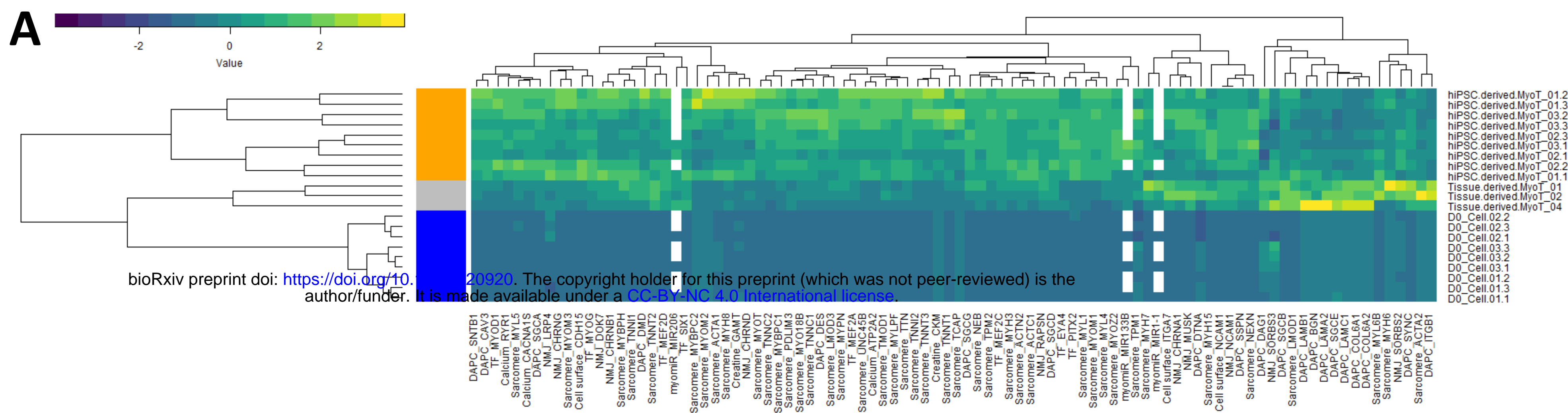

bioRxiv preprint doi: https://doi.org/10.1101/2020.01.20.20920. The copyright holder for this preprint (which was not peer-reviewed) is the author/funder. It is made available under a CC-BY-NC 4.0 International license.

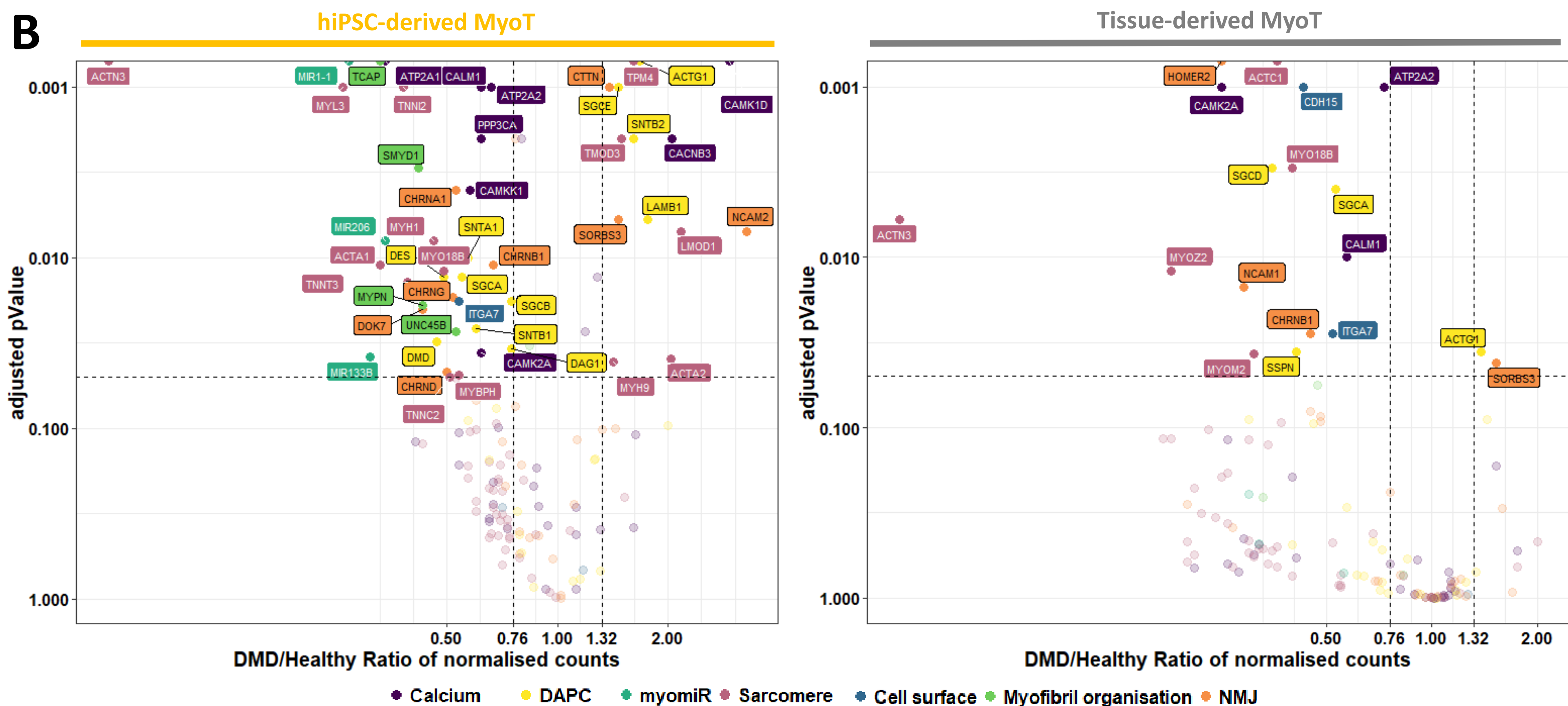

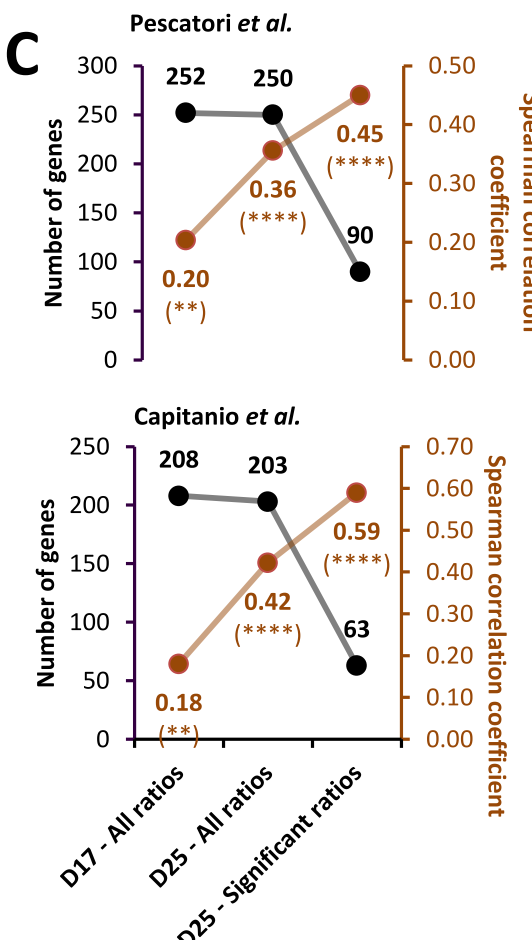

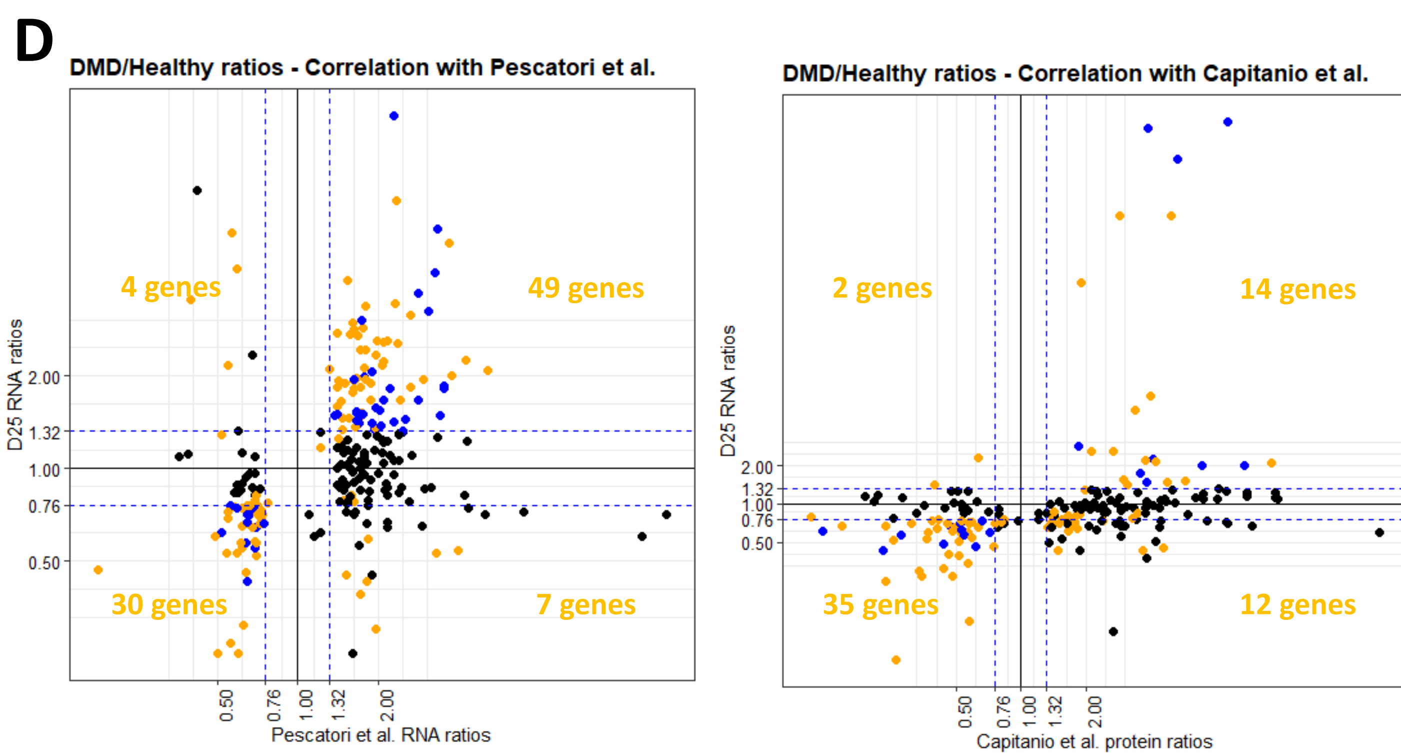

Figure 5

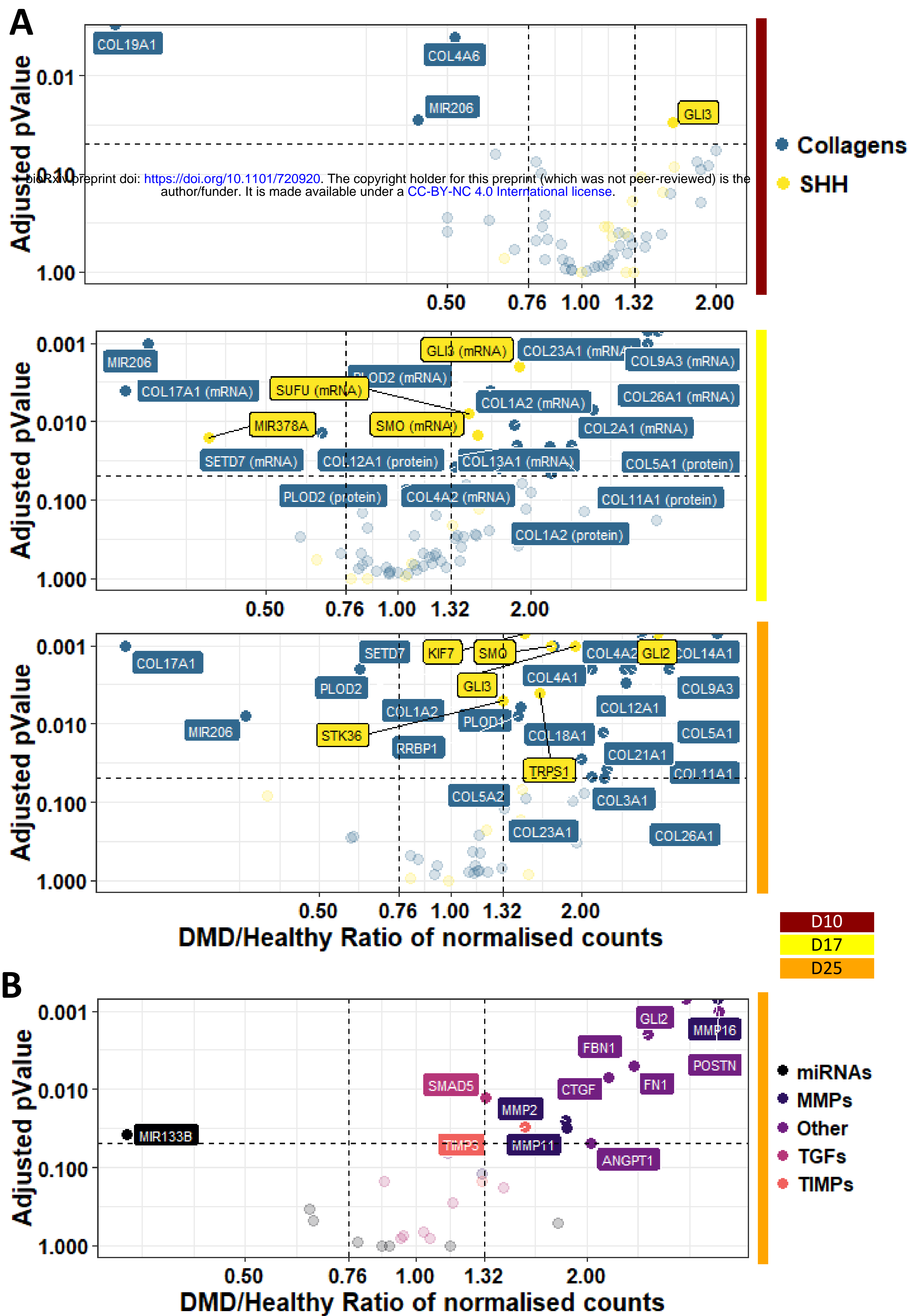

bioRxiv preprint doi: https://doi.org/10.1101/720920. The copyright holder for this preprint (which was not peer-reviewed) is the author/funder. It is made available under a CC-BY-NC 4.0 International license.

Figure 6

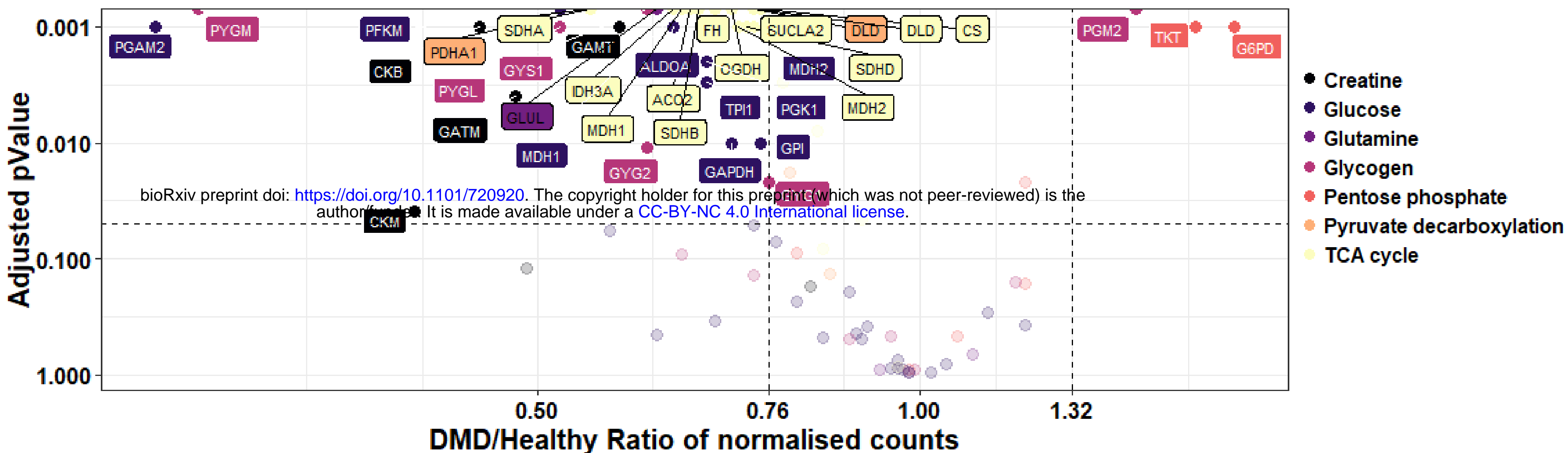

bioRxiv preprint doi: https://doi.org/10.1101/720920. The copyright holder for this preprint (which was not peer-reviewed) is the author/funder. It is made available under a CC-BY-NC 4.0 International license.

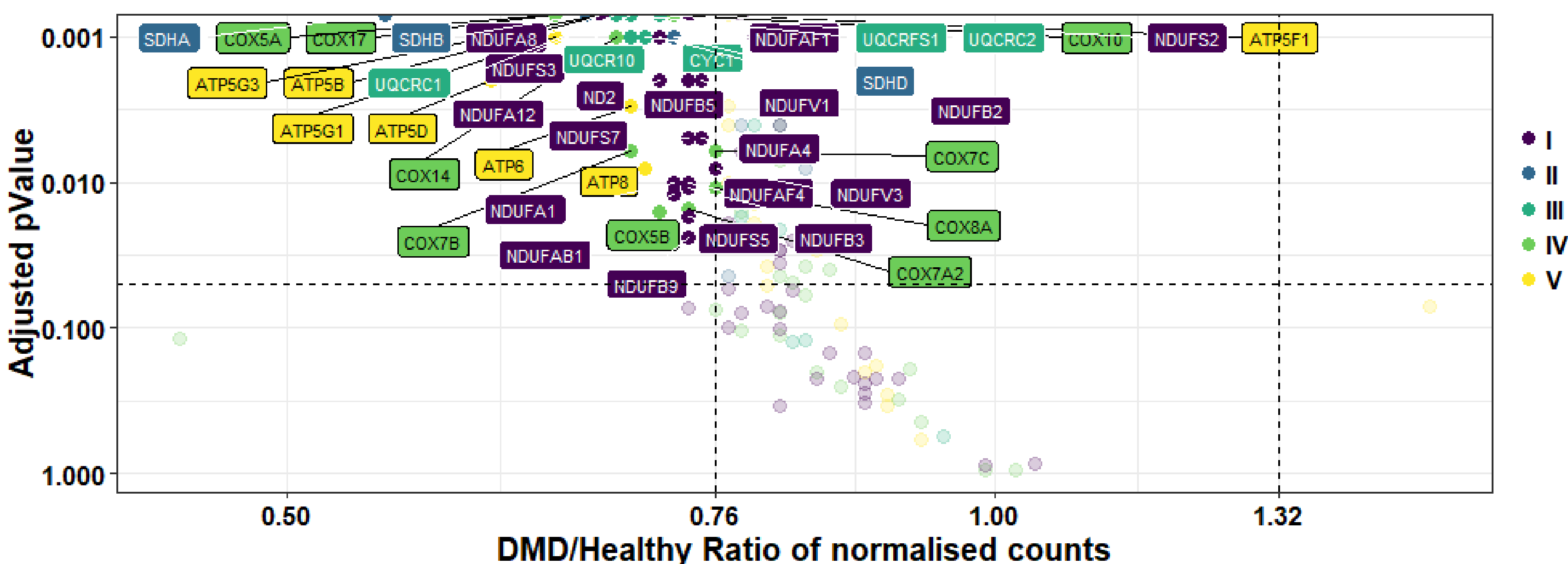

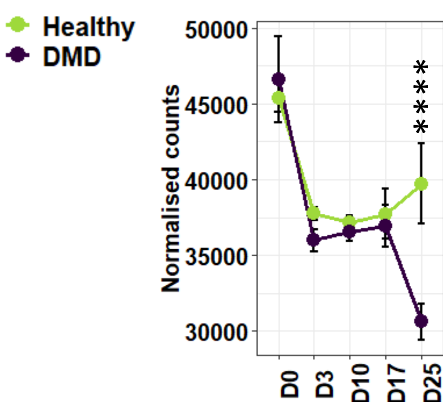

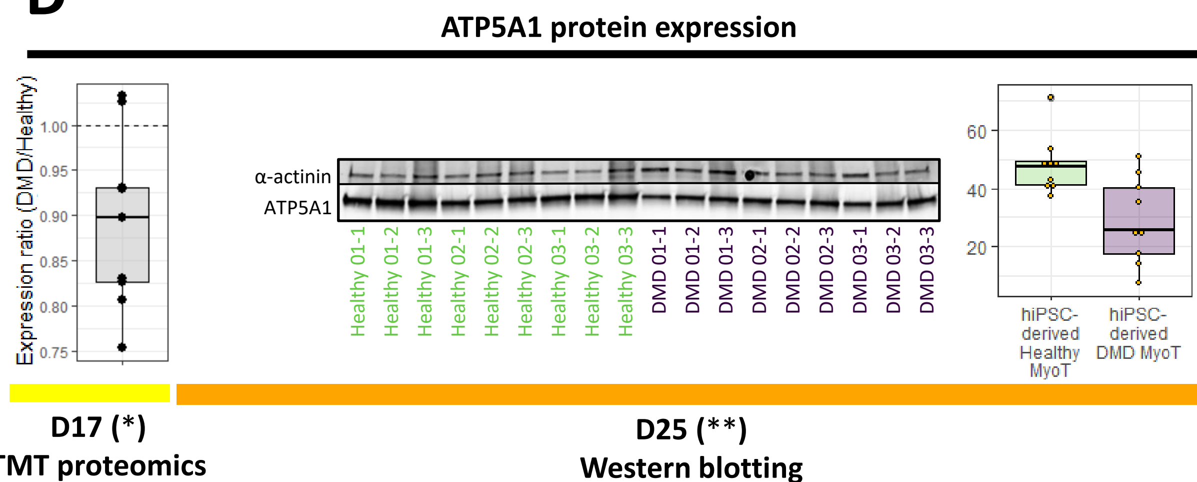

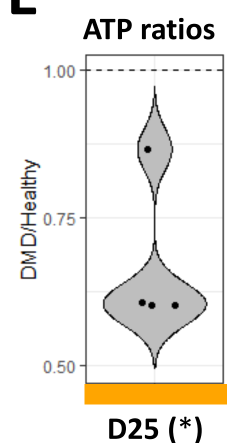

Figure 7

bioRxiv preprint doi: https://doi.org/10.1101/720920. The copyright holder for this preprint (which was not peer-reviewed) is the author/funder. It is made available under a CC-BY-NC 4.0 International license.